

## RESEARCH ARTICLE SUMMARY

## CELL CYCLE

# Chemically induced proximity reveals a Piezo-dependent meiotic checkpoint at the oocyte nuclear envelope

Chenshu Liu\* and Abby F. Dernburg\*

**INTRODUCTION:** Successful sexual reproduction requires the production of gametes, which are specialized cells that contain only a haploid set of chromosomes, or half the genome content of germline progenitor cells. This is achieved through meiosis, the specialized cell division in which the two copies of homologous chromosomes inherited from both parents are accurately segregated. During meiosis, homologous chromosomes must pair up along their lengths to enable genetic crossing-over, which is essential for accurate segregation. Physical pairing between homologs is usually stabilized by synapsis, in which a protein complex called the synaptonemal complex (SC) assembles between homologs along their lengths. Failure in synapsis can lead to chromosome missegregation and aneuploidy, a major cause of birth defects such as Down Syndrome. In diverse organisms, defects in synapsis can trigger apoptosis, but the mechanisms by which meiotic cells detect and respond to synapsis failure remain unclear.

**RATIONALE:** In *Caenorhabditis elegans*, defects in synapsis during meiosis result in a cell cy-

cle delay and eventually promote apoptosis of oocytes. Previous work revealed that this synapsis checkpoint depends on functional pairing centers (PCs), special regions near one end of each chromosome that interact with the nuclear envelope and promote homolog pairing and synapsis. In early meiotic prophase, the polo-like kinase PLK-2 is recruited to the PCs, where it plays essential roles in pairing and synapsis, in part by phosphorylating proteins at the nuclear envelope (NE). PLK relocates to the SC as chromosomes synapse. Synapsis defects result in prolonged association of PLK-2 with PCs and phosphorylation of NE proteins. To test whether the presence of PLK-2 at PCs acts as a signal that promotes apoptosis, we modified the auxin-inducible degradation (AID) system to create a chemically induced proximity (CIP) system. This enabled us to target PLK-2 to PCs in fully synapsed meiotic nuclei and to elucidate the signaling pathway leading to germline apoptosis.

**RESULTS:** We found that recruitment of PLK-2 to X chromosome PCs was sufficient to activate the synapsis checkpoint and induce apoptosis

of oocytes. Targeting PLK-2 to PCs also greatly prolonged the phosphorylation of lamin/LMN-1, which is normally phosphorylated by PLK-2 at meiotic entry to promote chromosome movement. The kinase activity of PLK-2 and phosphorylation of LMN-1 are both required to trigger apoptosis. Moreover, inducing dimerization of PLK-2 and LMN-1 also activated the synapsis checkpoint and bypassed the normal requirement for functional PCs. Recruiting PLK-2 to LMN-1 destabilized the nuclear lamina and caused increased deformation of oocyte NE. Unexpectedly, we found that mechanosensitive Piezo1/PEZO-1 channels localized to the oocyte NE and that PEZO-1 plays an essential role in the synapsis checkpoint.

**CONCLUSION:** We have developed a CIP system that is simple and effective in *C. elegans* and demonstrated its utility for subcellular relocalization of proteins. Using CIP, we have identified a key role for PLK-2 in a conserved meiotic checkpoint that enables oocytes to detect and respond to synapsis failures. When chromosomes fail to synapse, PLK-2 is retained at chromosome PCs, resulting in persistent phosphorylation of the nuclear lamin LMN-1. This weakens the lamina and triggers Piezo1/PEZO-1-dependent apoptosis of oocytes. Similar quality control mechanisms may ensure accurate meiotic chromosome segregation in diverse species. ■

The list of author affiliations is available in the full article online.

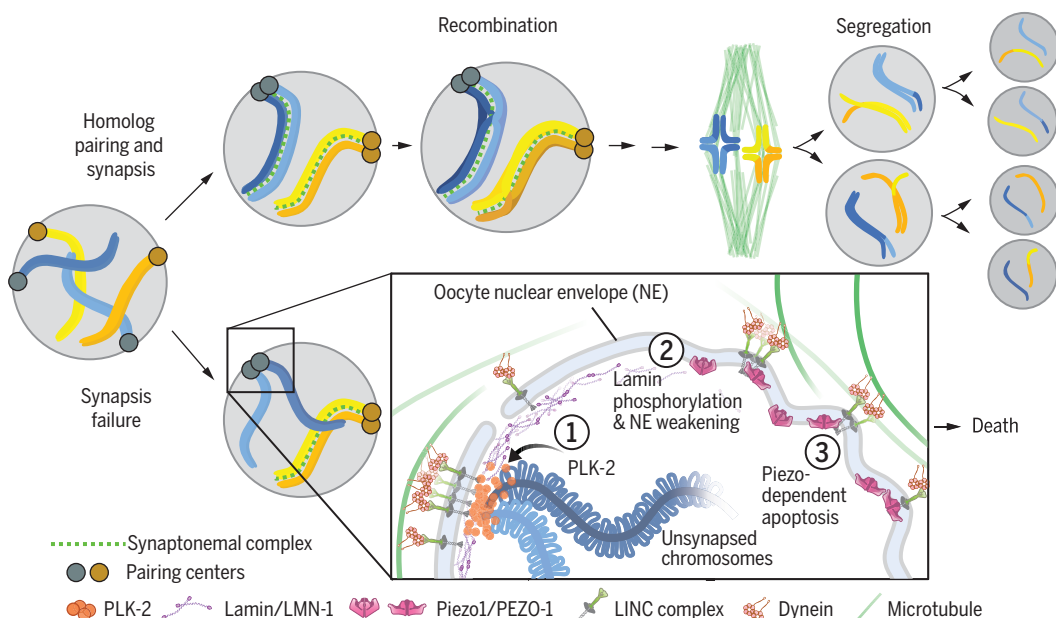
\*Corresponding author. Email: chenshu.liu@lehigh.edu (C.L.); afderenburg@berkeley.edu (A.F.D.)

Cite this article as C. Liu, A. F. Dernburg, *Science* **386**, eadm7969 (2024). DOI: 10.1126/science.adm7969

**S** READ THE FULL ARTICLE AT  
<https://doi.org/10.1126/science.adm7969>

## A Piezo-dependent checkpoint mechanism at the nuclear envelope monitors oocyte quality.

Pairing, synapsis, and recombination between homologous chromosomes are essential for accurate meiotic chromosome segregation. In *C. elegans*, failures in chromosome synapsis promote apoptosis of affected oocytes. After synapsis defects occur, PLK-2 persists at the pairing centers (step 1) and phosphorylates the nuclear lamin protein LMN-1 (step 2). This destabilizes the nuclear envelope and triggers PEZO-1/Piezo-dependent apoptosis (step 3). LINC complex, linker of nucleoskeleton and cytoskeleton complex.



## RESEARCH ARTICLE

## CELL CYCLE

# Chemically induced proximity reveals a Piezo-dependent meiotic checkpoint at the oocyte nuclear envelope

Chenshu Liu<sup>1,2,\*</sup> and Abby F. Dernburg<sup>1,2\*</sup>

Sexual reproduction relies on robust quality control during meiosis. Assembly of the synaptonemal complex between homologous chromosomes (synapsis) regulates meiotic recombination and is crucial for accurate chromosome segregation in most eukaryotes. Synapsis defects can trigger cell cycle delays and, in some cases, apoptosis. We developed and deployed a chemically induced proximity system to identify key elements of this quality control pathway in *Caenorhabditis elegans*. Persistence of the polo-like kinase PLK-2 at pairing centers—specialized chromosome regions that interact with the nuclear envelope—induced apoptosis of oocytes in response to phosphorylation and destabilization of the nuclear lamina. Unexpectedly, the Piezo1/PEZO-1 channel localized to the nuclear envelope and was required to transduce this signal to promote apoptosis in maturing oocytes.

**C**ellular surveillance mechanisms help to ensure accurate transmission of genetic information during mitosis and meiosis. In many eukaryotes, defects occurring during meiosis or gametogenesis can lead to cell cycle delay, cell death, or both. Although some of these pathways respond to unrepaired DNA damage (1, 2), additional checkpoints monitor meiosis-specific events such as synapsis, defined as the assembly of the synaptonemal complex (SC) between homologous chromosomes (3–6). In some organisms, apoptosis of germ cells in response to meiotic defects is sex-specific or sex-biased; for example, in mammals, defective spermatocytes are culled more stringently than oocytes (7, 8). This accounts for the sterility (azoospermia) of men carrying mutations in genes required for meiosis (9, 10) and may also contribute to the higher incidence of aneuploidy in human ova than in sperm (7, 11).

In the hermaphroditic nematode *Caenorhabditis elegans*, meiotic defects can trigger cell cycle checkpoints in both spermatogenesis and oogenesis. Defective oocytes, but not spermatoocytes, also frequently undergo apoptosis, even though both types of gametes are produced in the same tissue in hermaphrodites (12). A substantial fraction of oocytes normally undergo “physiological” apoptosis, i.e., even in the absence of apparent meiotic defects (13), but unrepaired DNA damage or failures in homologous

chromosome synapsis result in increased apoptosis and preferential culling of the affected oocytes (4). Several factors are specifically required for apoptosis in response to DNA damage or synapsis defects. The former depends on canonical DNA damage sensing and signaling factors, whereas the synapsis checkpoint depends on functional pairing centers (PCs)—special regions on each chromosome that mediate nuclear envelope (NE) attachment and promote homolog pairing and synapsis during early meiotic prophase (4, 14–17). This synapsis checkpoint also requires the meiotic kinase PLK-2 (polo-like kinase 2) and the widely conserved AAA+ adenosine triphosphatase (ATPase) PCH-2 (4, 18). Yet how meiotic nuclei detect and respond to unsynapsed chromosomes remains unclear.

In early meiosis, the meiotic kinases CHK-2 and PLK-2 are recruited to chromosome PCs by zinc finger proteins that bind to dispersed DNA sequence motifs in these chromosome regions and interact with the NE (14, 15, 19). These kinases phosphorylate SUN-1, a component of the linker of nucleoskeleton and cytoskeleton (LINC) complex that promotes chromosome movement along the NE during early prophase (18, 20). PLK-2 also phosphorylates the lamin protein LMN-1, which makes the lamina more labile and facilitates chromosome movement along the nuclear surface (21). Upon completion of synapsis, PLK-2 relocates from PCs to the SC (18, 22, 23). Synapsis defects result in prolonged association of PLK-2 with PCs and extended phosphorylation of SUN-1 and LMN-1 (24–26). PLK-2 is also required for the synapsis checkpoint (18). These findings led us to test whether the persistence of PLK-2 at PCs might signal the presence of unsynapsed chromosomes.

## Results

**A chemically induced proximity system in *C. elegans*** To test whether PLK-2 at chromosome PCs affects meiotic progression or apoptosis, we adapted the auxin-inducible degradation (AID) system to control protein localization. In plants, the phytohormone auxin [indole acetic acid (IAA)] triggers binding of target proteins carrying a “degron” sequence by the F-box protein TIR1, which interacts with Cullin1 and associated proteins to form an SCF E3 ubiquitin ligase complex (27). Expression of TIR1 from *Arabidopsis thaliana* in *C. elegans* results in auxin-induced degradation of proteins tagged with degron sequences derived from *Arabidopsis* IAA17 or other TIR1 targets (28, 29). We modified a *C. elegans AtTIR1* transgene to incorporate two amino acid substitutions that abrogate the interaction between TIR1 and Cullin 1 and thereby block degradation of degron-tagged proteins (30, 31) (Fig. 1A). We expressed this mutated TIR1 (TIR1<sup>CIP</sup>) fused to mRuby, a monomeric red fluorescent protein, and confirmed that in the presence of auxin, this fluorescent fusion protein was recruited to proteins fused with a degron (e.g., PLK-2::AID) (fig. S1 and movie S1) but did not result in their degradation. Notably, this recruitment appears to be reversible (fig. S2).

This should be a broadly useful system for inducible dimerization and proximity in *C. elegans*. Auxin is nontoxic, inexpensive, and water-soluble, and it can penetrate the worm eggshell and cuticle at all stages of development, in contrast to larger dimerizers such as rapamycin analogs (32–39). Many degron-tagged alleles of endogenous genes have already been generated and can be readily exploited for dimerization experiments. Although auxin has some physiological effects on *C. elegans*, including a small life-span extension and endoplasmic reticulum (ER) stress resistance (40, 41), these do not generally affect the interpretation of experiments involving short-term manipulation of protein localization.

### PLK-2 at PCs is sufficient to induce apoptosis of oocytes in late prophase

PCs are specialized chromosome regions required for homolog pairing and synapsis during meiosis in *C. elegans*. They span large genomic regions and are functionally defined by the presence of many binding sites that recruit one of four paralogous zinc finger proteins to each of the six chromosomes (14, 15). HIM-8 associates with the X chromosome PC throughout meiotic prophase (14). To enable auxin-inducible targeting of PLK-2 to the X chromosome PC, we generated a strain expressing PLK-2::TIR1<sup>CIP</sup> and degron-tagged HIM-8 (AID::HIM-8). Neither of these detectably perturbed the function of the tagged protein (table S1). In animals exposed to auxin, PLK-2 was detected at X chromosome PCs throughout meiotic prophase,

<sup>1</sup>California Institute for Quantitative Biosciences (QB3) and Department of Molecular and Cell Biology, University of California Berkeley, Berkeley, CA, USA. <sup>2</sup>Division of Biological Systems and Engineering, Lawrence Berkeley National Laboratory, Berkeley, CA, USA.

†Present address: Department of Biological Sciences, Lehigh University, Bethlehem, PA, USA.

\*Corresponding author. Email: chenshu.liu@lehigh.edu (C.L.); afderenburg@berkeley.edu (A.F.D.)

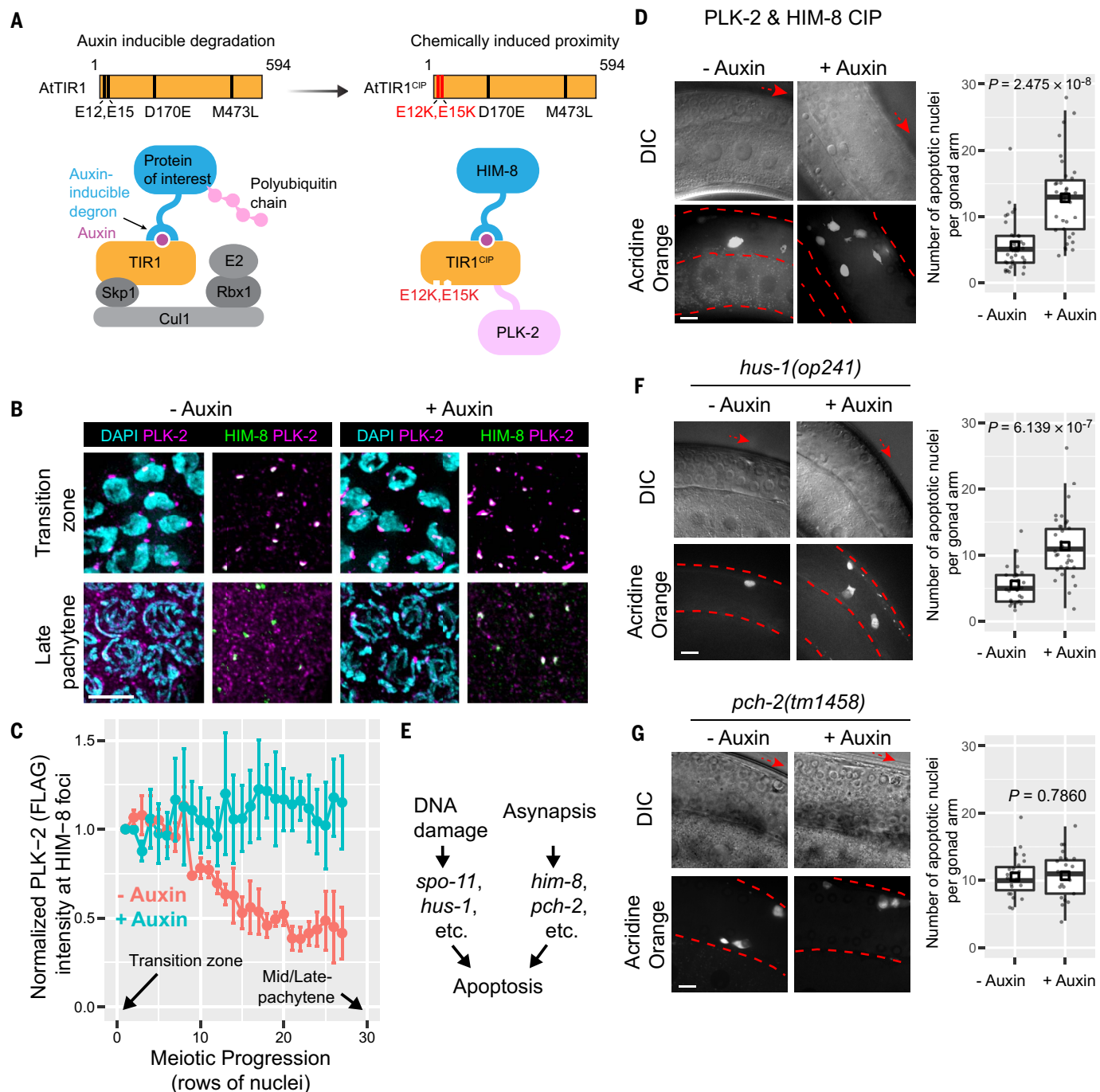


**Fig. 1. Recruitment of PLK-2 to X chromosome pairing centers activates the synapsis checkpoint.** (A) The auxin-inducible degradation system was adapted to create an inducible dimerization system by incorporating two amino acid substitutions that abrogate binding between TIR1 and other E3 ligase components. Amino acid substitutions relative to the wild-type *A. thaliana* TIR1 sequence are indicated. The D170E and M473L substitutions enhance the affinity of TIR1 for auxin, whereas the E12K and E15K mutations disrupt its ability to form an SCF complex (28, 30). Single-letter abbreviations for the amino acid residues are as follows: D, Asp; E, Glu; K, Lys; L, Leu; M, Met. (B) Immunofluorescence showing PLK-2 localization in relation to

X chromosome pairing centers (PCs), marked by HIM-8, in transition-zone and late-pachytene nuclei, with or without ( $\pm$ ) auxin treatment. Scale bar, 5  $\mu$ m. (C) Quantification of PLK-2 (FLAG) intensity at HIM-8 foci during meiotic progression. Means  $\pm$  SEM were calculated based on data from three animals. (D, F, and G) Representative examples of differential interference contrast (DIC) and acridine orange (AO) fluorescence images of germ lines from the specified genotypes,  $\pm$  auxin treatment. Scale bars, 10  $\mu$ m. Box plots show quantification of apoptotic nuclei based on AO staining. Each dot represents one animal. Medians (black crossbars) and means (black boxes) are shown. (E) Schema showing two meiotic checkpoints that lead to apoptosis.

whereas in control animals, PLK-2 was only enriched at these sites in “transition zone” (Leptotene-zygote) and early-pachytene nuclei (Fig. 1, B and C) (22, 23). Dimerization be-

tween PLK-2 and HIM-8 did not cause synapsis defects (fig. S3).

To quantify germline apoptosis, we stained live worms with the vital dye acridine orange

(AO), which specifically labels apoptotic cell corpses in the germ line (12, 42–46). After imaging of intact animals with a spinning disk confocal microscope, we counted the number

of fluorescent corpses in each arm of the gonad. Ectopic targeting of PLK-2 to X chromosome PCs significantly increased the number of apoptotic nuclei in the germ line (Fig. 1D). Increased apoptosis was also detected when only one of the two *plk-2* copies was fused to *TIR1<sup>CIP</sup>*, demonstrating that PLK-2 recruitment to the X chromosome PC is sufficient to trigger oocyte death even when the untagged protein localizes to the SC (fig. S4).

Either unrepaired DNA damage or unsynapsed chromosomes can induce germline apoptosis (4) (Fig. 1E). HUS-1, an essential component of the DNA damage checkpoint, was dispensable for apoptosis resulting from recruitment of PLK-2 to X chromosome PCs, whereas PCH-2, which is required for the synapsis checkpoint, was essential (Fig. 1, F and G). Thus, ectopic targeting of PLK-2 to PCs triggers apoptosis via the synapsis checkpoint.

#### Phosphorylation of the nuclear lamina promotes apoptosis

To test whether the kinase activity of PLK-2 is required to trigger apoptosis, we introduced an active-site mutation into the *plk-2::TIR1<sup>CIP</sup>* fusion gene using CRISPR-Cas9 (21, 23) (fig. S5). Recruitment of this catalytically inactive PLK-2<sup>K65M</sup> to HIM-8 did not induce germline apoptosis (Fig. 2A), indicating that kinase activity is required for the role of PLK-2 in this checkpoint response.

Several serine and threonine residues in the sole *C. elegans* nuclear lamin protein LMN-1 have been identified as PLK-2-dependent phosphorylation sites (18, 20, 21, 47). A phosphospecific antibody against LMN-1 pSer32 revealed that this site is normally phosphorylated upon meiotic entry and becomes dephosphorylated by mid-pachytene (21). Ectopic recruitment of PLK-2 to X chromosome PCs greatly extended the region of the gonad containing pSer32-positive meiotic nuclei (Fig. 2B). We thus wondered whether lamin phosphorylation by PLK-2 is required to induce apoptosis. A mutant allele of LMN-1 in which eight phosphorylation sites are mutated to alanine, LMN-1<sup>8A</sup> impairs lamin disassembly in both mitosis and meiosis (21, 47). This allele prevented induction of germline apoptosis when PLK-2 was recruited to X chromosome PCs (Fig. 2A), indicating that LMN-1 phosphorylation is required for the checkpoint response.

We thus tested whether ectopic targeting of PLK-2 to the nuclear lamina is sufficient to induce germline apoptosis. Indeed, auxin-induced dimerization of PLK-2::TIR1<sup>CIP</sup> and LMN-1::AID (45) resulted in increased germline apoptosis that was independent of HUS-1 and DNA damage (Fig. 2C and fig. S6). Moreover, we found that recruitment of PLK-2 to the nuclear lamina triggered apoptosis even in a strain lacking all four PC zinc finger proteins (Fig. 2D). Thus, the crucial role of PCs in the synapsis checkpoint is

to recruit PLK-2 to the NE, where it phosphorylates LMN-1.

#### Recruiting PLK-2 to LMN-1 destabilizes the nuclear lamina

We further investigated the effects of recruiting PLK-2 to the nuclear lamina through immunofluorescence analysis. After PLK-2 recruitment, staining of epitope-tagged LMN-1 showed strongly reduced fluorescence (a “dark zone”) throughout much of meiotic prophase, indicating that the abundance of LMN-1 at the NE was reduced or that the protein was extracted during tissue preparation (Fig. 3A). This dark zone was not observed when catalytically inactive PLK-2 (PLK-2<sup>K65M</sup>) was recruited to LMN-1, indicating that it is a consequence of LMN-1 phosphorylation (Fig. 3B and fig. S7). To determine whether this weakening of the nuclear lamina might be a cause or a consequence of apoptosis, we introduced a mutation in CED-4 (an ortholog of mammalian Apaf-1), which is required for germline apoptosis (4, 48, 49). In this *ced-4* null mutant, ectopic targeting of PLK-2 to LMN-1 still destabilized the nuclear lamina, indicated by a reduction in LMN-1 immunofluorescence (Fig. 3C). Thus, lamin instability triggered by proximity between PLK-2 and LMN-1 is not a consequence of germline apoptosis. HUS-1 was dispensable for this LMN-1 dark zone, indicating that this response is also independent of the DNA damage checkpoint (Fig. 3D). Depleting LMN-1 even in the absence of functional PCs also induced HUS-1-independent apoptosis (Fig. 2E), indicating that weakening of the nuclear lamina through LMN-1 phosphorylation or depletion is sufficient to activate the synapsis checkpoint.

Mutation or depletion of essential SC components results in asynapsis and increased germline apoptosis (fig. S8) (24, 50–52). We depleted SYP-2 using RNA interference [*syp-2(RNAi)*] to induce asynapsis and found that this also resulted in an extended dark zone of LMN-1 (Fig. 4A). This did not depend on HUS-1 (Fig. 4B) but was abolished in the absence of PLK-2 activity (*plk-2<sup>K65M</sup>*) and in the *lmn-1<sup>8A</sup>* mutant (Fig. 4, C to E), indicating that PLK-2-dependent phosphorylation of LMN-1 is a normal consequence of asynapsis. Germline apoptosis in response to SYP-2 depletion was suppressed by the *lmn-1<sup>8A</sup>* mutation (fig. S9), further indicating that phosphorylation of the lamina by PLK-2 is integral to the synapsis checkpoint.

The pachytene region of the germ line in wild-type animals typically contains several nuclei with polarized chromosome morphology more typical of the transition zone (19, 53, 54). These nuclei often showed synapsis defects and weak immunofluorescence of LMN-1 (fig. S10, A to D). Moreover, the appearance of such nuclei depended on the kinase activity of PLK-2

(fig. S10, E and F). Thus, these nuclei displayed hallmarks of synapsis checkpoint activation.

Depletion of LMN-1 is sufficient to cause polarized nuclear morphology even in the absence of functional chromosome pairing centers (45). Together with data presented here and observations from numerous other studies (19, 24, 25, 50, 51), this indicates that the primary driver of polarized—or crescent-shaped—nuclear morphology normally observed during leptotene-zygote is the disruption of the nuclear lamina through phosphorylation or lamin depletion, rather than NE attachment or movement of chromosomes.

#### The mechanosensitive channel Piezo1/PEZO-1 is required for the synapsis checkpoint

Depletion of LMN-1 in the *C. elegans* germ line reduces nuclear stiffness and results in deformation of the NE in response to forces mediated by cytoplasmic dynein and LINC complexes (45, 55). Recruitment of PLK-2 to the nuclear lamina also led to increased deformation of the nuclear surface (Fig. 5, A and B, and movie S2). This suggests that phosphorylation of the lamina makes the NE more readily deformable, presumably in response to intracellular forces (45, 55, 56).

Piezo proteins form cation channels in the plasma membrane that open in response to mechanical deformation (57–60). *C. elegans* has only one Piezo protein, PEZO-1 (61, 62). Green fluorescent protein (GFP)-tagged PEZO-1 localizes to plasma membranes throughout the *C. elegans* germ line. We were intrigued by the appearance of faint GFP::PEZO-1 fluorescence surrounding oocyte nuclei (61) and confirmed that a subset of PEZO-1 localizes to the NE of maturing oocytes in two different fluorescently tagged strains (Fig. 5, C and D, and fig. S11, A to C), most prominently in the late-pachytene region of the gonad, where apoptosis occurs (Fig. 5C and fig. S11, A and B). We thus wondered whether PEZO-1 might respond to deformations of the NE during oogenesis. In *pezo-1* mutants, ectopic recruitment of PLK-2 to the nuclear lamina did not lead to increased germline apoptosis (Fig. 5E). Moreover, recruiting PLK-2 to the nuclear lamina failed to trigger apoptosis when wild-type animals were exposed to Yoda1, a Piezo1 agonist that keeps the channel in an open state, disrupting Piezo signaling (61, 63). Yodal exposure had no effect on germline apoptosis in *pezo-1* mutants, indicating that it acts through PEZO-1 (fig. S11D). These results indicate that the ion channel function of PEZO-1 is required for the synapsis checkpoint. Elevated germline apoptosis triggered by lamin depletion or asynapsis was also abolished in *pezo-1* null mutants (Fig. 5E). We further observed that the lamin dark zone caused by recruiting PLK-2 to LMN-1 did not require PEZO-1 (fig. S11E). Thus, the role of PEZO-1 in the synapsis checkpoint is downstream of lamin phosphorylation and destabilization.

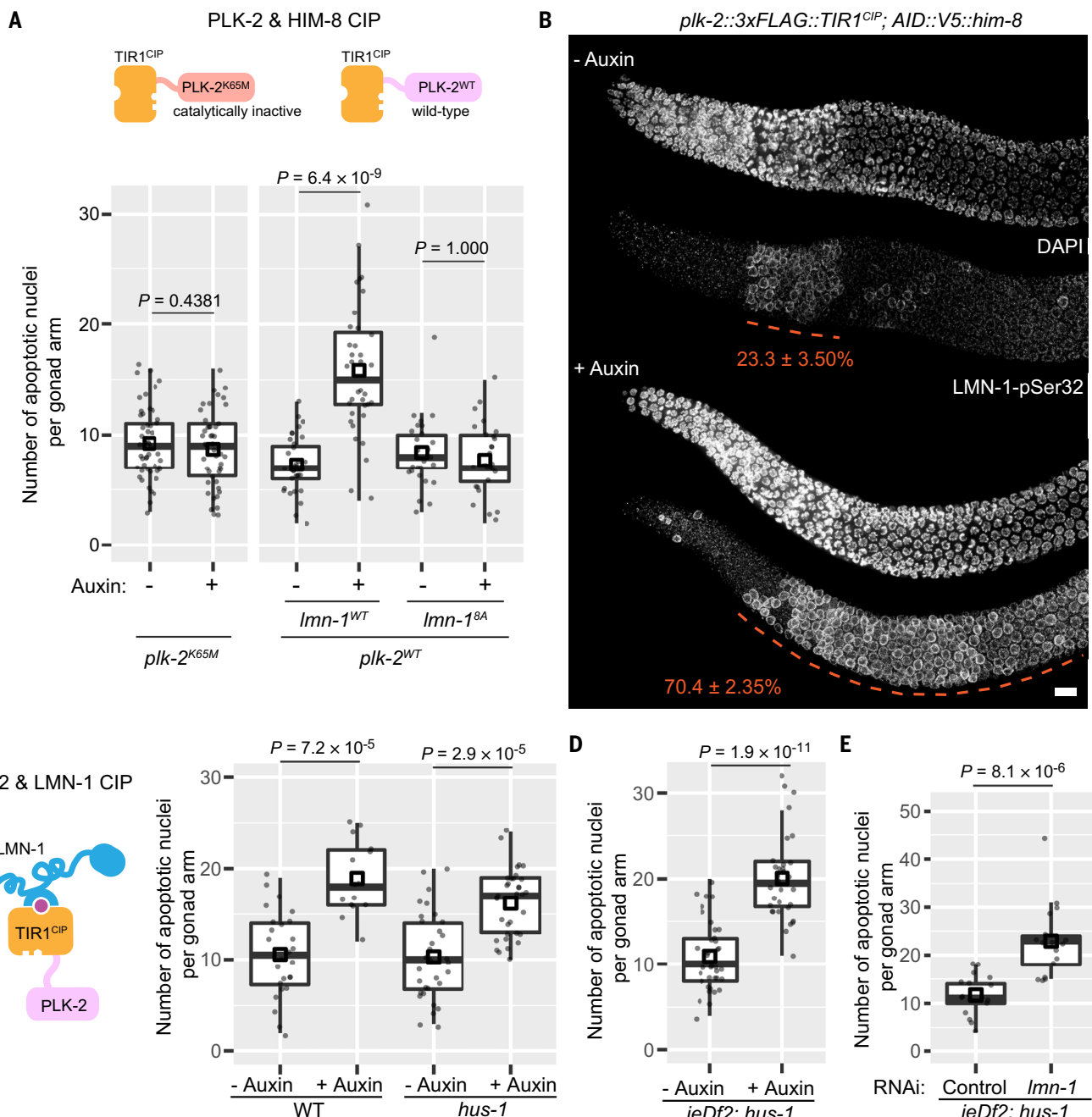


**Fig. 2. Phosphorylation of the nuclear lamina by PLK-2 promotes apoptosis.**

(A) Apoptosis in response to asynapsis requires PLK-2 kinase activity and LMN-1 phosphorylation. Recruitment of catalytically inactive PLK-2<sup>K65M</sup> to the X chromosome PCs fails to trigger elevated apoptosis. WT, wild-type. (B) Immunofluorescence showing extended region of meiotic nuclei with phosphorylated LMN-1-Ser32. Scale bar, 10 μm. Red dashed lines indicate regions with nuclei having phosphorylated LMN-1-Ser32. Numbers (means ± SD) indicate the percent of all meiotic prophase nuclei before late-pachytene that stain positive for phosphorylated LMN-1-Ser32.  $P < 2.2 \times 10^{-16}$  by two-proportions z test. In total, 790 nuclei (- Auxin) and 703 nuclei (+ Auxin) were scored. DAPI, 4',6-diamidino-2-phenylindole. (C) Recruiting PLK-2 to LMN-1 triggers apoptosis independent of HUS-1. (D) Recruitment of PLK-2 to LMN-1 is sufficient to trigger the synapsis checkpoint in the absence of functional PCs. *ieDf2* is a deletion of the four genes encoding essential PC proteins (18). *hus-1* is required for the DNA damage checkpoint. (E) Depletion of LMN-1 by RNAi also induces elevated apoptosis independent of HUS-1. For (A), (C), (D), and (E), box plots show quantification of apoptotic nuclei based on AO staining. Each dot represents one animal. Medians (black crossbars) and means (black boxes) are shown.

#### Asynapsis induces PCH-2-dependent redistribution of PEZO-1 at the NE

PEZO-1 localizes to both the plasma membrane and the NE, raising the question of whether the role of PEZO-1 in the synapsis checkpoint de-

pends on channels within the nuclear membrane. After SYP-2 depletion, recruitment of PLK-2 to the nuclear lamina, or depletion of LMN-1 by RNAi, GFP::PEZO-1 fluorescence at the NE became concentrated at a few puncta

(Fig. 6A and fig. S12). These PEZO-1 foci co-localized with cytoplasmic dynein (DHC-1) and LINC complexes, which were also clustered in oocytes affected by asynapsis (Fig. 6B). The distribution of PEZO-1 at the plasma membrane

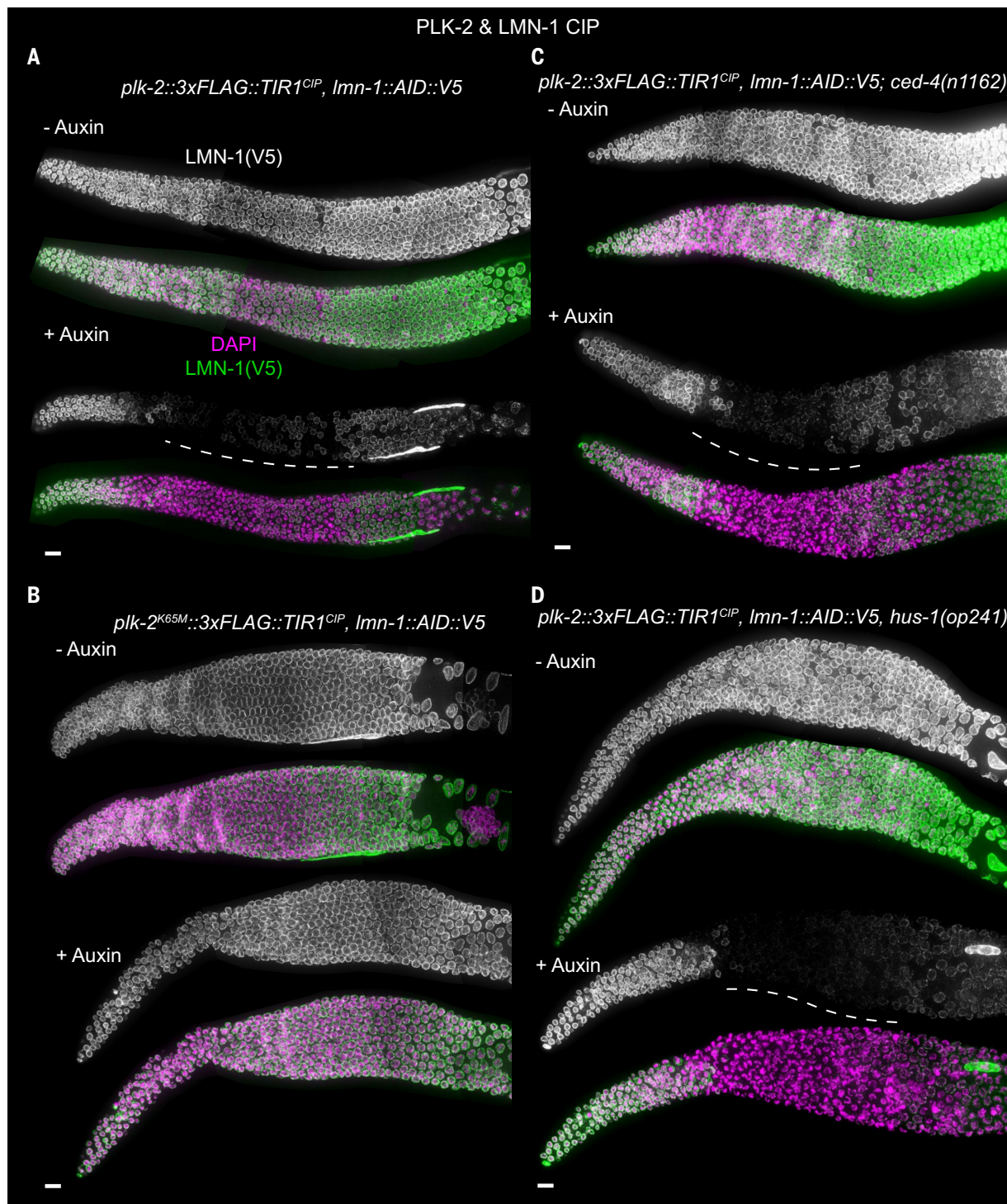
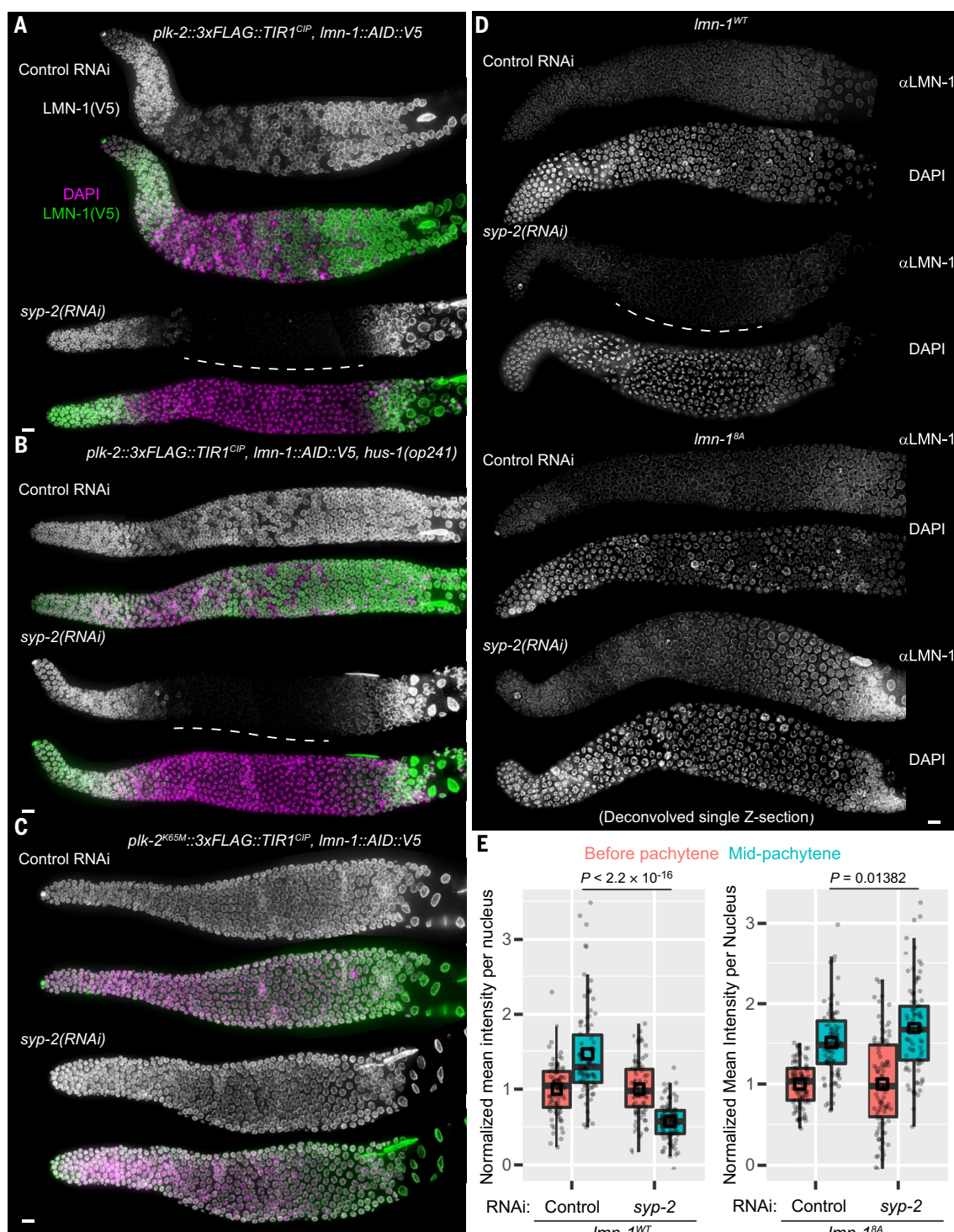


**Fig. 3. Recruitment of PLK-2 to LMN-1 weakens the nuclear lamina.**

Representative maximum-intensity projections of immunofluorescence images of gonads showing LMN-1::V5 (grayscale images and green in composite images) and DNA (DAPI, magenta in composite images). Scale bars, 10  $\mu\text{m}$ . (A to D) Each panel represents a different genotype. The lamin dark zone is indicated with dashed lines. LMN-1::V5 staining is still observed in the large, polyplloid gonadal sheath cells that surround the germline cells. For (A), zero out of five control (-Auxin) gonads imaged displayed a lamin dark zone, whereas six out of six

imaged gonads had a lamin dark zone under the "+ Auxin" condition. For (B), zero out of six imaged gonads had a lamin dark zone under the "- Auxin" condition, and zero out of six imaged gonads had a lamin dark zone under the "+ Auxin" condition. For (C), zero out of three imaged gonads had a lamin dark zone under the "- Auxin" condition, whereas three out of three imaged gonads had a lamin dark zone under the "+ Auxin" condition. For (D), zero out of three imaged gonads had a lamin dark zone under the "- Auxin" condition, whereas four out of four imaged gonads had a lamin dark zone under the "+ Auxin" condition.

**Fig. 4. Asynapsis triggers PLK-2-dependent weakening of the nuclear lamina.** (A to C) Representative images showing dissected gonads from animals treated with control RNAi or *syp-2(RNAi)*, stained for epitope (V5)-tagged LMN-1 (grayscale images and green in composite images) and DNA (DAPI, magenta in composite images). Images are maximum-intensity projections. Scale bars, 10  $\mu$ m. A lamin dark zone (dashed white lines) can be observed in WT (A) or in the absence of HUS-1 (B) but not in the absence of PLK-2 kinase activity (C). For (A), zero out of five imaged gonads had a lamin dark zone under the "Control RNAi" condition, whereas five out of five imaged gonads had a lamin dark zone under the "*syp-2(RNAi)*" condition. For (B), zero out of five imaged gonads had a lamin dark zone under the "Control RNAi" condition, and six out of six imaged gonads had a lamin dark zone under the "*syp-2(RNAi)*" condition. For (C), zero out of six imaged gonads had a lamin dark zone under the "Control RNAi" condition, and zero out of five imaged gonads had a lamin dark zone under the "*syp-2(RNAi)*" condition. (D) Representative immunofluorescence of dissected gonads stained for endogenous LMN-1 in WT or *lmn-1<sup>8A</sup>* background. Single optical sections from deconvolved data stacks are shown. Scale bar, 10  $\mu$ m. The dark zone is more



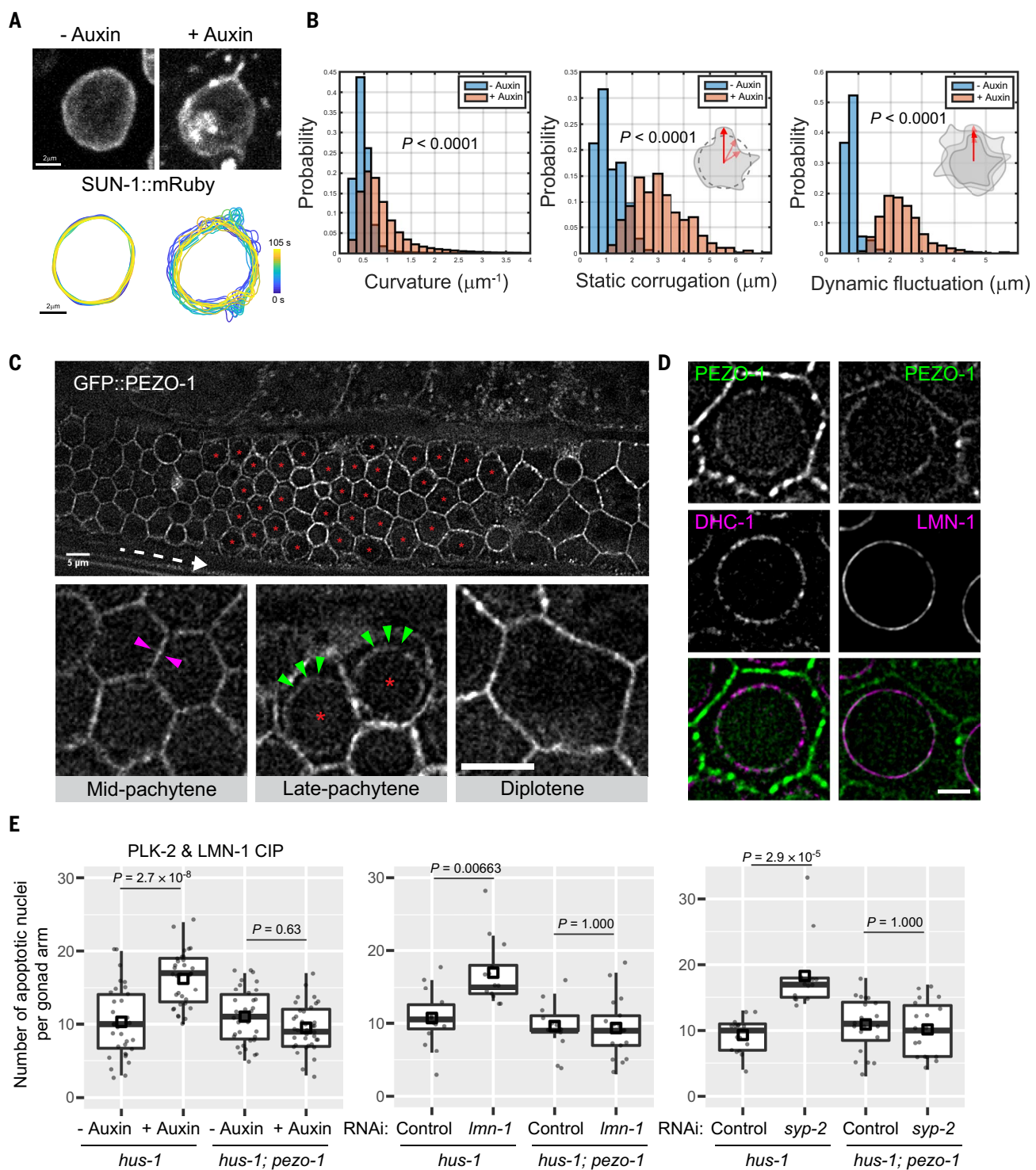
pronounced in animals expressing epitope-tagged LMN-1. (E) Box plots show quantification of mean endogenous LMN-1 intensity per nucleus, normalized against endogenous LMN-1 intensity before pachytene. Each dot represents one nucleus. Medians (black crossbars) and means (black boxes) are shown. For each condition, 30 meiotic nuclei per stage from each of three animals were measured [Control RNAi or *syp-2(RNAi)*]. *P* values were calculated using the two-sample *t* test.

did not change perceptibly in response to synapsis checkpoint activation.

SUN-1 and ZYG-12 constitute a LINC complex that transduces cytoskeletal forces to the NE throughout meiotic prophase (16, 45, 64). Depletion of SYP-2, which results in asynapsis,

failed to trigger apoptosis when SUN-1 was also depleted, indicating that SUN-1 is essential for the synapsis checkpoint (Fig. 6C). A separation-of-function missense mutation, *sun-1(jf18)*, perturbs mechanotransduction by SUN-1-ZYG-12 LINC complexes, which results

in extensive nonhomologous synapsis (65, 66). This leads to an increase in apoptosis that depends on double-strand breaks generated by SPO-11, indicating that it is triggered by the DNA damage checkpoint (66). We found that depletion of SYP-2 in *sun-1(jf18)* homozygotes

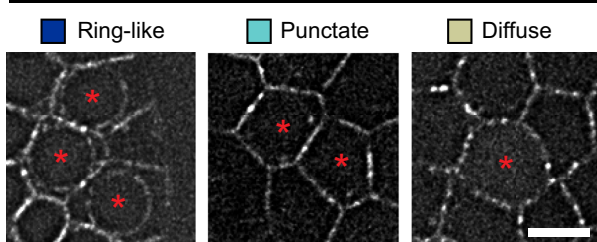


**Fig. 5. The mechanosensitive channel PEZO-1 localizes to the NE and is required for the synapsis checkpoint.** (A) Still frames from live imaging of late-pachytene nuclei expressing SUN-1::mRuby as an NE marker, without or with auxin treatment to recruit PLK-2 to the nuclear lamina. Images are maximum-intensity projections. Scale bar, 2  $\mu$ m. Nuclear contours are aligned by centroids and color-coded by time. (B) Histograms for nuclear contours' curvature, static corrugation, and dynamic fluctuation (see materials and methods for more details).  $P$  values were computed using the two-sample  $t$  test. (C) Live imaging of an adult gonad expressing GFP::PEZO-1 (single optical section). Dashed white arrow indicates the direction of meiotic progression. Red asterisks indicate meiotic

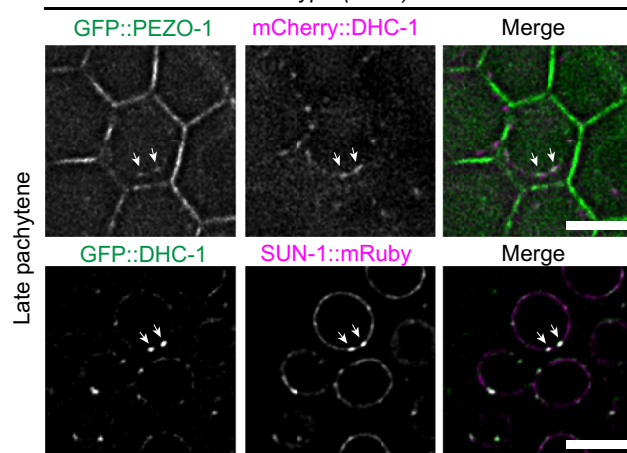
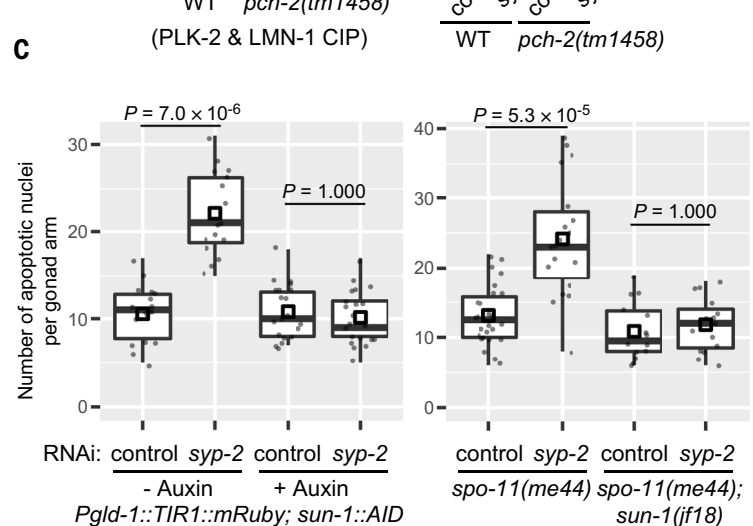
cells with "ringlike" localization of GFP::PEZO-1 at the nuclear periphery. Magenta arrowheads indicate GFP fluorescence at the plasma membrane. Green arrowheads indicate GFP signals at the nuclear periphery. Scale bars, 5  $\mu$ m. (D) Live-imaging stills (single optical section) of late-pachytene nuclei, showing localization of PEZO-1 and NE markers dynein (mCherry::DHC-1) or GFP::LMN-1 (21, 28, 45). GFP::PEZO-1 is in the left column and mScarlet::PEZO-1 in the right column. Scale bar, 2  $\mu$ m. (E) PEZO-1 is required for CIP-induced or asynapsis-triggered apoptosis. Box plots show quantification of apoptotic nuclei based on AO staining. Each dot represents one animal. Medians (black crossbars) and means (black boxes) are shown.

**A**

GFP::PEZO-1

**B**

syp-2(RNAi)

**C****Fig. 6. Asynapsis induces PCH-2-dependent PEZO-1 redistribution at the NE.**

(A) (Left) Single confocal optical sections of images from live animals, illustrating three classes of GFP::PEZO-1 localization and their relative abundance among all late-pachytene nuclei. Scale bar, 5  $\mu$ m. (Right) Percentages were calculated with pooled data from at least three animals per condition.  $P < 2 \times 10^{-16}$  (WT – auxin versus WT + auxin),  $P = 0.98$  (pch-2 – auxin versus pch-2 + auxin),  $P < 2 \times 10^{-16}$  [WT; control versus WT; syp-2(RNAi)],  $P = 0.88$  [pch-2; control versus pch-2; syp-2(RNAi)], all computed using pairwise comparison of proportions of nuclei with

ringlike GFP::PEZO-1 localization (adjusted by the Benjamini-Hochberg method). (B) Representative images of live animals showing PEZO-1 foci that overlap with dynein (mCherry::DHC-1) and LINC complexes (SUN-1::mRuby) after syp-2(RNAi)-induced asynapsis. Images are single confocal optical sections of late-pachytene nuclei in live animals. Scale bars, 5  $\mu$ m. (C) Mechanotransduction mediated by SUN-1 is required for the synapsis checkpoint. Box plots show quantification of apoptotic nuclei based on AO staining. Each dot represents one animal. Medians (black crossbars) and means (black boxes) are shown.

did not lead to SPO-11-independent apoptosis (Fig. 6C), providing further evidence that LINC-mediated mechanotransduction is important for the synapsis checkpoint.

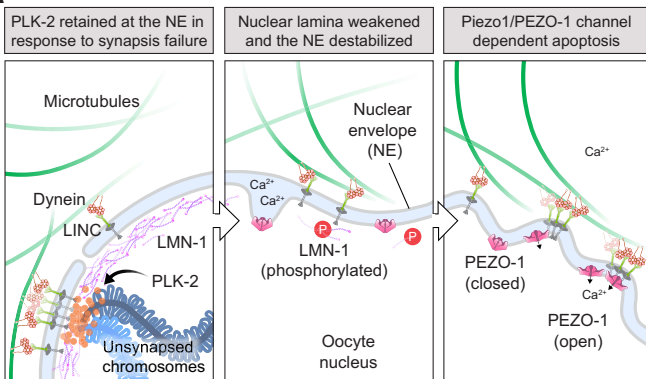
The AAA+ ATPase PCH-2 (also known as Pch2 or TRIP13 in other organisms) plays a conserved but enigmatic role in meiotic checkpoints (67–74). Disruption of pch-2 did not affect the localization of PLK-2 or lamin phosphorylation under conditions that trigger the synapsis checkpoint (figs. S13 and S14). However, the redistribution of PEZO-1 at the NE in response to asynapsis was abrogated in pch-2 mutants (Fig. 6A and fig. S12). Thus, PCH-2 is required for the redistribution or remodeling of PEZO-1 at the NE. These observations further support a role for PEZO-1 at the NE in apoptosis.

## Discussion

Chemically induced proximity (CIP) is a versatile experimental tool that takes advantage

of cell-permeant small molecules (75). Several CIP approaches for protein dimerization have been engineered for use in cultured cells (31, 76). Their application in model organisms has been more limited, owing to the challenges of delivering the molecular ligands and their impact on physiology. By repurposing the versatile AID system, we developed a CIP system that is easy to use and can also capitalize on the plethora of *C. elegans* strains expressing degron-tagged endogenous proteins. This approach can enable (i) visualization of endogenous proteins that are sensitive to constitutive fluorescent protein tagging in live animals (e.g., using fluorescently tagged TIR1<sup>CIP</sup>) and (ii) ectopic recruitment and relocalization of proteins of interest. Using this system, we have elucidated a quality control mechanism acting at the NE during meiosis, in which unsynapsed chromosomes lead to destabilization of the lamina and PEZO-1-dependent apoptosis (Fig. 7).

Cell nuclei experience mechanical forces from both intracellular and extracellular sources (77–80). Piezo1 has previously been implicated in transducing extracellular force to mediate changes in heterochromatin stiffness within the nucleus (81). This pathway involves Piezo1-mediated release of intracellular calcium from the ER and leads to a reduction in lamina-associated, H3K9me3-enriched heterochromatin, resulting in nuclear softening. Patch-clamp experiments on isolated nuclei have detected stretch-activated  $\text{Ca}^{2+}$  currents (82–84), suggesting the presence of mechanosensitive channels at the NE, but these were never identified. Our findings implicate Piezo channels in transducing intracellular forces and triggering apoptosis. PEZO-1 may be activated by deformation of the nuclear membrane, or the channels may be mechanically coupled to LINC complexes or other cytoskeletal components, as has been reported for Piezo1 at the plasma membrane

**A**

**Fig. 7. Model of a Piezo-channel-dependent checkpoint mechanism that monitors oocyte quality at the NE. (A)** In response to synapsis defects, PLK-2 is retained at the NE by binding to PCs. Phosphorylation of LMN-1 causes NE destabilization and PEZO-1-dependent apoptosis. **(B)** Schematic summary of the

(59, 85, 86). Opening of the channels may lead to Ca<sup>2+</sup> release from the perinuclear space or the ER lumen, thereby triggering downstream proapoptotic pathways (Fig. 7) (87–89). Spontaneous, or “physiological,” apoptosis of *C. elegans* oocytes results from a hydraulic instability that amplifies oocyte volume differences during a period of rapid cell growth, causing some cells to grow and survive while others shrink, leading to cell death (90). We thus speculate that PEZO-1-mediated signaling may promote apoptosis by predisposing affected cells to shrink and die during oocyte maturation.

Treatment of *C. elegans* with the Piezo1 agonist Yoda1 abrogated the synapsis checkpoint, similarly to loss-of-function mutations in *pezo-1*. Similarly, the role of PEZO-1 in *C. elegans* ovulation was impaired by Yoda1 (61). Although it may be counterintuitive for a channel agonist to phenocopy a loss-of-function mutation, this may simply reflect a key role for ion transients in signaling apoptosis.

In most eukaryotes, telomeres interact with LINC complexes during early meiotic prophase and drive chromosomal motion that promotes homolog pairing (91). This evolutionarily conserved function can also be mediated by centromeres, as in *Drosophila* (92), or by PCs, as in *C. elegans* (91). Our findings reveal that these interactions between chromosomes and the NE have an additional role in triggering a meiotic checkpoint through lamin phosphorylation. In *C. elegans*, homologous synapsis occurs independently of DNA double-strand breaks or crossover (CO) formation. However, in most eukaryotes, SC assembly is coupled to the formation of crossover precursors. Monitoring of SC assembly thus serves as a crossover assurance mechanism. We suggest that a role for interactions between chromosomes and the NE in checkpoint signaling may also be widely conserved. In mice, the kinase Cdk2 localizes to both telomeres and CO sites and

is essential to link telomeres to the NE to form the meiotic bouquet (93, 94). Vertebrate CDKs phosphorylate nuclear lamins to disassemble the NE in mitosis (95–98), and Cdk2 may thus also modulate NE dynamics during meiotic prophase. Double-strand break formation, which is essential for CO formation, is important for timely bouquet resolution (99). The bouquet stage is also prolonged in *Symp3* mutants, which fail to complete synapsis (100). Additionally, mouse spermatocytes lacking the meiosis-specific lamin C2 show highly elevated apoptosis (101). Although this may be a consequence of meiotic defects arising from the absence of meiotic lamins, it is also possible that perturbation of the lamina is a trigger for apoptosis, as we have found in *C. elegans*.

In other organisms, oocytes also experience a range of mechanical forces during meiosis and oogenesis (45). In mammals, oocytes are produced in the ovary of a developing fetus and then arrest at the dictyate (diplotene) stage for as long as several decades before resuming meiosis (102). Mechanical forces have been implicated in maintenance of this long arrest and are likely to contribute to oocyte maturation and follicle selection as well as maintenance of ovarian reserve (103–105). Piezo2 is detected in human ovarian follicles (<https://www.proteinatlas.org/ENSG00000154864-PIEZO2/tissue/ovary#img>, from v23.0.proteinatlas.org), suggesting a potential role for these channels in mechanical regulation of dormancy and maturation (106). Our work reveals an important role for Piezo channels in oocyte quality control, with potential implications for age-related decline in oocyte quality and *in vitro* gametogenesis.

## Materials and methods

### Generation of worm strains

All *C. elegans* strains were maintained at 20°C under standard conditions (107). All alleles were generated using CRISPR-Cas9 genome

editing (Alt-R CRISPR-Cas9 gRNA products, IDT), as previously described (45). Details of alleles generated in this study are listed in table S2. A complete list of *C. elegans* strains used and generated in this study is also provided in table S3. Custom-designed crRNAs targeting genes of interest were purchased from IDT. These sequences, as well as the sequences of double-stranded DNA repair templates (gBlocks from IDT) and single-stranded DNA repair template for *dpy-10* (IDT) can be found in table S4. A repair template for editing the endogenous *plk-2* gene to express *PLK-2::3xFLAG::TIR1<sup>CIP</sup>* was assembled into a pCR-Blunt backbone using Gibson Assembly (NEB) and confirmed using Sanger sequencing and whole-plasmid Nanopore sequencing (Primordium). Templates and CRISPR RNAs to create additional transgenes or alleles were designed and injected but resulted in gene silencing, including the insertion of *TIR1<sup>CIP</sup>::V5* at the 5' end of the endogenous *him-8* gene, insertion of a *TIR1<sup>CIP</sup>::V5::him8* transgene into the universal MosSCI site *oxTII79* II, and replacing *mRuby* in *ieSi38[sun-1p::TIR1::mRuby::sun-1 3'UTR, Cbr-unc-119(+)]IV* with *V5::him-8*.

### Fertility and viability

Brood size, embryonic viability, and males among the self-progeny of individual hermaphrodites were quantified as previously described (45).

### AO staining

Quantification of apoptosis by AO staining was carried out as previously described (45, 46) with minor modifications. AO staining solution was freshly prepared by diluting a 10-mg/ml stock solution (Invitrogen A-3568) 1:200 into M9 buffer. Age-matched adult hermaphrodites were picked to the middle of a lawn of *E. coli* OP50 on fresh plates. Two ml of staining solution was gently pipetted onto each plate until the entire surface (including the OP50 lawn) was covered. When necessary, animals were repositioned using a pipette onto the OP50 lawn to ensure active feeding behavior and efficient AO uptake. Plates were incubated for 1 hour at room temperature in the dark. Worms were then washed off the plate with M9 buffer, transferred to low-retention 1.5-ml tubes (Fisherbrand) and pelleted by a low-speed spin (10 s) in a tabletop mini centrifuge. They were washed with 600 µl M9 buffer. Pelleting and washing were repeated for a total of three washes, after which worms were transferred to fresh plates to recover at room temperature for 45 min in the dark. They were mounted on agarose pads and imaged within 1 hour of the end of the recovery period. Low retention pipette tips (Fisherbrand) were used throughout the washing process.

We note that the baseline level of apoptosis (in the absence of synapsis checkpoint activation) varied by nearly 2.5-fold (from 5.5 to 13 nuclei per gonad arm) across different experiments

described here (see data S1). Some of this variation is related to differences in reproductive age (108), because some experiments (e.g., those involving RNA interference) required up to 36 hours of treatment and incubation before imaging. Some may reflect strain-specific differences in the dynamics of apoptosis and engulfment. Due to this variability, the effects of mutations or other perturbations were always based on comparison to appropriate age-matched controls in the same experiment.

#### RNAi, auxin and Yoda1 treatment, and apoptosis assays

Depletion of gene products by feeding RNAi was carried out as previously described (45). Bacterial strains from the Ahringer RNAi feeding library (109, 110) carrying RNAi clones targeting *syp-2* and *lmn-1* were validated by whole-plasmid Nanopore sequencing (Primordium) (table S5).

NGM worm plates containing 2 mm indole acetic acid (IAA, auxin) were prepared and used as previously described (45). Worms were transferred to plates containing auxin 12 to 16 hours after the L4 stage and treated for 12 to 24 hours, depending on the specific experimental needs. Treatment time was identical among all genotypes/groups in the same set of experiment. The time required for efficient CIP recruitment and the duration of auxin treatment in each experiment were both determined empirically. For experiments using the Piezo agonist Yoda1 (Tocris # 5586), the compound was dissolved in DMSO (Amresco #WN182) to make a 2.5 mM stock. This solution was diluted 1:125 into NGM medium to make plates containing 20  $\mu$ M Yoda1 (61). An equal volume of DMSO was added to control plates (61). For all experiments involving RNAi, auxin or Yoda1 treatment, and/or AO staining, apoptosis was scored within 36 hours after the L4 stage to minimize any age-related effects on apoptosis (108, 111).

#### Immunofluorescence

Immunofluorescence was carried out as previously described (45, 112). For imaging of GFP::PEZO-1 in dissected gonads (e.g., fig. S11C), worms were dissected in detergent-free egg buffer to preserve GFP::PEZO-1 at NE in fixed samples. The following antibodies were used: anti-FLAG (mouse M2, F3165, 1:400), anti-V5 (mouse, P/N 46-0705, Invitrogen, 1:400), anti-V5 (rabbit, 1:400), anti-GFP (mouse monoclonal, Roche, 1:400), anti-SYP-1 [goat, affinity purified, 1:400 (18)], anti-SYP-2 (rabbit, affinity purified, 1:1000), anti-HTP-3 [chicken, 1:400 (113)], anti-HTP-3 [guinea pig, 1:400 (113)], anti-HIM-8 [rat, 1:400 (14)], anti-HIM-8 (rabbit polyclonal, affinity purified, SDIX, SDQ2975, 1:1000), anti-NPP-7 (rabbit polyclonal, affinity purified, SDIX, SDQ0870, 1:1,000), anti-LMN-1 (rat, #3933, 1:200, a gift from Yosef Gruenbaum), anti-LMN-1-pSer32

[rabbit, 1:10 with pre-adsorption, a gift from Verena Jantsch (21)], and secondary antibodies conjugated to Alexa 488, Cy3, or Cy5/AF647 (Jackson ImmunoResearch or Life Technologies; 1:400). For all imaging of fixed gonads, at least 15 animals for each experimental condition were dissected and visually examined by fluorescence microscopy. Because little variation was observed in the staining pattern among individuals, unless otherwise noted, at least three germ lines were imaged as multichannel three-dimensional (3D) stacks for each experimental condition or genotype. All images of fixed samples were acquired using a DeltaVision Elite system (GE) equipped with a 100  $\times$  1.45 NA oil-immersion objective (Olympus) or a Marianas/SoRa spinning disc confocal microscope (Intelligent Imaging Innovations, Inc.) at ambient temperature (21°C), using a 100  $\times$  1.46 NA oil immersion objective. Images were deconvolved using the SoftWoRx Suite (Applied Precision, GE) or the proprietary Microvolution software in Slidebook (Intelligent Imaging Innovations, Inc.) respectively. Identical imaging parameters (e.g., illumination power and exposure time) were used for all samples in the same experiment. All fixed gonads were imaged as 3D image stacks with 0.2  $\mu$ m z-spacing. Maximum intensity projections of deconvolved 3D images were generated using Fiji unless otherwise noted. Image stitching and figure composition was performed using Adobe Illustrator.

#### Live imaging

Live imaging was performed as previously described (45). Immobilized worms mounted on agarose pads were imaged with a Marianas/SoRa spinning disk confocal microscope (Intelligent Imaging Innovations, Inc.) at ambient temperature (21°C), using a 100  $\times$  1.46 NA oil immersion objective. For apoptosis assays, differential interference contrast (DIC) and 488-nm laser excitation were used to image and score AO-positive apoptotic nuclei in the germ line. Three-dimensional images of the germ line were acquired as Z-stacks of 26 focal planes at intervals of 0.5  $\mu$ m, which spanned approximately half of the total thickness of tissue. For dynamics of the NE marker SUN-1::mRuby, 3D image stacks were acquired every 5 s for a total duration of 5 min, with 12 Z-sections at intervals of 0.5  $\mu$ m per time point. 488- or 561-nm excitation lasers were used with identical parameters between control and experimental samples. Deconvolved 3D images were assembled using Fiji and Illustrator (Adobe) for figures, unless otherwise noted.

#### Image analysis

Fluorescence intensity of PLK-2(FLAG) at HIM-8 foci or fluorescence intensity of LMN-1(V5) of each nucleus was manually segmented and measured from additive projection images after background subtraction using Fiji. For endogenous

LMN-1 staining, due to limited signal-to-noise ratio, fluorescence intensity was measured along the circumference of the cross section of each nucleus with background subtraction in Fiji. Percentages of nuclei positive for LMN-1-pSer32 staining or types of distribution of fluorescently tagged PEZO-1 were measured manually. Quantification of the fraction of nuclei with complete synapsis was carried out as previously described (45). For curvature analysis,  $n = 11$  (- auxin) or 15 (+ auxin) late-pachytene nuclei (pooled from at least four animals in each condition) were analyzed for the deformation of NE contours, which was manually segmented for at least 20 consecutive frames acquired every 5 s using Fiji and subsequently processed in MATLAB (R2023a, Mathworks) (114). Curvature measurement at any given moment for each nucleus over the whole tracked duration were combined for plotting the histogram. Pixels that lie along NE contours were converted from Cartesian coordinates to polar coordinates. “Static corrugation” is the standard deviation over all polar angles of the contour radius for each nucleus at one time point. The histogram shows the distribution of this value for all time points. “Dynamic fluctuation” is the standard deviation of radii at each angular position for all time points in a series. The histogram shows the distribution of this value for all angles.

#### Statistics

All statistical analyses were carried out using RStudio (Version 1.2.5033) or MATLAB (R2023a, Mathworks). All *P* values were calculated using the Mann-Whitney test or two-sample *t* test when analyzing the number of apoptotic nuclei per gonad arm using AO assays (Figs. 1, D to G; 2, A, and C to E; 5E; 6C; and figs. S4, S9, and S11D). Key statistical test results are included in figure legends. All detailed statistics can be found in data S1.

#### REFERENCES AND NOTES

1. M. Di Giacomo et al., Distinct DNA-damage-dependent and -independent responses drive the loss of oocytes in recombination-defective mouse mutants. *Proc. Natl. Acad. Sci. U.S.A.* **102**, 737–742 (2005). doi: [10.1073/pnas.0406212102](https://doi.org/10.1073/pnas.0406212102); pmid: [15640358](https://pubmed.ncbi.nlm.nih.gov/15640358/)
2. F. Baudat, K. Manova, J. P. Yuen, M. Jaslin, S. Keeney, Chromosome synapsis defects and sexually dimorphic meiotic progression in mice lacking Spo11. *Mol. Cell* **6**, 989–998 (2000). doi: [10.1016/S1097-2765\(00\)00098-8](https://doi.org/10.1016/S1097-2765(00)00098-8); pmid: [1106739](https://pubmed.ncbi.nlm.nih.gov/1106739/)
3. T. Odorosio, T. A. Rodriguez, E. P. Evans, A. R. Clarke, P. S. Burgoyne, The meiotic checkpoint monitoring synapsis eliminates spermatocytes via p53-independent apoptosis. *Nat. Genet.* **18**, 257–261 (1998). doi: [10.1038/ng0398-257](https://doi.org/10.1038/ng0398-257); pmid: [9500548](https://pubmed.ncbi.nlm.nih.gov/9500548/)
4. N. Bhalla, A. F. Dernburg, A conserved checkpoint monitors meiotic chromosome synapsis in *Caenorhabditis elegans*. *Science* **310**, 1683–1686 (2005). doi: [10.1126/science.1117468](https://doi.org/10.1126/science.1117468); pmid: [16339446](https://pubmed.ncbi.nlm.nih.gov/16339446/)
5. O. Rog, A. F. Dernburg, Chromosome pairing and synapsis during *Caenorhabditis elegans* meiosis. *Curr. Opin. Cell Biol.* **25**, 349–356 (2013). doi: [10.1016/j.ceb.2013.03.003](https://doi.org/10.1016/j.ceb.2013.03.003); pmid: [23578368](https://pubmed.ncbi.nlm.nih.gov/23578368/)
6. S. G. Gordon, O. Rog, Building the synaptonemal complex: Molecular interactions between the axis and the central

- region. *PLOS Genet.* **19**, e1010822 (2023). doi: [10.1371/journal.pgen.1010822](https://doi.org/10.1371/journal.pgen.1010822); pmid: [37471284](https://pubmed.ncbi.nlm.nih.gov/37471284/)
7. P. A. Hunt, T. J. Hassold, Sex matters in meiosis. *Science* **296**, 2181–2183 (2002). doi: [10.1126/science.1071907](https://doi.org/10.1126/science.1071907); pmid: [12077403](https://pubmed.ncbi.nlm.nih.gov/12077403/)
  8. Y. Huang, I. Roig, Genetic control of meiosis surveillance mechanisms in mammals. *Front. Cell Dev. Biol.* **11**, 1127440 (2023). doi: [10.3389/fcell.2023.1127440](https://doi.org/10.3389/fcell.2023.1127440); pmid: [36910159](https://pubmed.ncbi.nlm.nih.gov/36910159/)
  9. S. Z. Jan et al., Distinct prophase arrest mechanisms in human male meiosis. *Development* **145**, dev160614 (2018). doi: [10.1242/dev.160614](https://doi.org/10.1242/dev.160614); pmid: [29540502](https://pubmed.ncbi.nlm.nih.gov/29540502/)
  10. D. Topping et al., Synaptic defects at meiosis I and non-obstructive azoospermia. *Hum. Reprod.* **21**, 3171–3177 (2006). doi: [10.1093/humrep/del281](https://doi.org/10.1093/humrep/del281); pmid: [16861745](https://pubmed.ncbi.nlm.nih.gov/16861745/)
  11. C. Charalambous, A. Webster, M. Schuh, Aneuploidy in mammalian oocytes and the impact of maternal ageing. *Nat. Rev. Mol. Cell Biol.* **24**, 27–44 (2023). doi: [10.1038/s41580-022-00517-3](https://doi.org/10.1038/s41580-022-00517-3); pmid: [36068367](https://pubmed.ncbi.nlm.nih.gov/36068367/)
  12. A. Jaramillo-Lambert, Y. Haryagaya, J. Vitt, A. Villeneuve, J. Engebrecht, Meiotic errors activate checkpoints that improve gamete quality without triggering apoptosis in male germ cells. *Curr. Biol.* **20**, 2078–2089 (2010). doi: [10.1016/j.cub.2010.10.008](https://doi.org/10.1016/j.cub.2010.10.008); pmid: [20970339](https://pubmed.ncbi.nlm.nih.gov/20970339/)
  13. S. A. Raiders, M. D. Eastwood, M. Bacher, J. R. Priess, Binucleate germ cells in *Caenorhabditis elegans* are removed by physiological apoptosis. *PLOS Genet.* **14**, e1007417 (2018). doi: [10.1371/journal.pgen.1007417](https://doi.org/10.1371/journal.pgen.1007417); pmid: [30024879](https://pubmed.ncbi.nlm.nih.gov/30024879/)
  14. C. M. Phillips et al., HIM-8 binds to the X chromosome pairing center and mediates chromosome-specific meiotic synapsis. *Cell* **123**, 1051–1063 (2005). doi: [10.1016/j.cell.2005.09.035](https://doi.org/10.1016/j.cell.2005.09.035); pmid: [16360035](https://pubmed.ncbi.nlm.nih.gov/16360035/)
  15. C. M. Phillips, A. F. Dernburg, A family of zinc-finger proteins is required for chromosome-specific pairing and synapsis during meiosis in *C. elegans*. *Dev. Cell* **11**, 817–829 (2006). doi: [10.1016/j.devcel.2006.09.020](https://doi.org/10.1016/j.devcel.2006.09.020); pmid: [1714157](https://pubmed.ncbi.nlm.nih.gov/1714157)
  16. A. Sato et al., Cytoskeletal forces span the nuclear envelope to coordinate meiotic chromosome pairing and synapsis. *Cell* **139**, 907–919 (2009). doi: [10.1016/j.cell.2009.10.039](https://doi.org/10.1016/j.cell.2009.10.039); pmid: [19913287](https://pubmed.ncbi.nlm.nih.gov/19913287/)
  17. O. Rog, A. F. Dernburg, Direct Visualization Reveals Kinetics of Meiotic Chromosome Synapsis. *Cell Rep.* **10**, 1639–1645 (2015). doi: [10.1016/j.celrep.2015.02.032](https://doi.org/10.1016/j.celrep.2015.02.032); pmid: [25772351](https://pubmed.ncbi.nlm.nih.gov/25772351/)
  18. N. C. Harper et al., Pairing centers recruit a Polo-like kinase to orchestrate meiotic chromosome dynamics in *C. elegans*. *Dev. Cell* **21**, 934–947 (2011). doi: [10.1016/j.devcel.2011.09.001](https://doi.org/10.1016/j.devcel.2011.09.001); pmid: [22018922](https://pubmed.ncbi.nlm.nih.gov/22018922/)
  19. Y. Kim, N. Kostow, A. F. Dernburg, The Chromosome Axis Mediates Feedback Control of CHK-2 to Ensure Crossover Formation in *C. elegans*. *Dev. Cell* **35**, 247–261 (2015). doi: [10.1016/j.devcel.2015.09.021](https://doi.org/10.1016/j.devcel.2015.09.021); pmid: [26506311](https://pubmed.ncbi.nlm.nih.gov/26506311/)
  20. S. Labella, A. Woglar, V. Jantsch, M. Zetka, Polo kinases establish links between meiotic chromosomes and cytoskeletal forces essential for homolog pairing. *Dev. Cell* **21**, 948–958 (2011). doi: [10.1016/j.devcel.2011.07.011](https://doi.org/10.1016/j.devcel.2011.07.011); pmid: [22018921](https://pubmed.ncbi.nlm.nih.gov/22018921/)
  21. J. Link et al., Transient and Partial Nuclear Lamina Disruption Promotes Chromosome Movement in Early Meiotic Prophase. *Dev. Cell* **45**, 212–225.e7 (2018). doi: [10.1016/j.devcel.2018.03.018](https://doi.org/10.1016/j.devcel.2018.03.018); pmid: [29689196](https://pubmed.ncbi.nlm.nih.gov/29689196/)
  22. D. Patabhiraman, B. Roelens, A. Woglar, A. M. Villeneuve, Meiotic recombination modulates the structure and dynamics of the synaptonemal complex during *C. elegans* meiosis. *PLOS Genet.* **13**, e1006670 (2017). doi: [10.1371/journal.pgen.1006670](https://doi.org/10.1371/journal.pgen.1006670); pmid: [28339470](https://pubmed.ncbi.nlm.nih.gov/28339470/)
  23. J. N. Brandt, K. A. Hussey, Y. Kim, Spatial and temporal control of targeting Polo-like kinase during meiotic prophase. *J. Cell Biol.* **219**, e202006094 (2020). doi: [10.1083/jcb.202006094](https://doi.org/10.1083/jcb.202006094); pmid: [32997737](https://pubmed.ncbi.nlm.nih.gov/32997737/)
  24. T. Bohr, G. Ashley, E. Eggleston, K. Firestone, N. Bhalla, Synaptonemal Complex Components Are Required for Meiotic Checkpoint Function in *Caenorhabditis elegans*. *Genetics* **204**, 987–997 (2016). doi: [10.1534/genetics.116.191494](https://doi.org/10.1534/genetics.116.191494); pmid: [27605049](https://pubmed.ncbi.nlm.nih.gov/27605049/)
  25. M. Castellano-Pozo et al., Surveillance of cohesin-supported chromosome structure controls meiotic progression. *Nat. Commun.* **11**, 4345 (2020). doi: [10.1038/s41467-020-18219-9](https://doi.org/10.1038/s41467-020-18219-9); pmid: [32859945](https://pubmed.ncbi.nlm.nih.gov/32859945/)
  26. W. Zhang et al., HAL-2 promotes homologous pairing during *Caenorhabditis elegans* meiosis by antagonizing inhibitory effects of synaptonemal complex precursors. *PLOS Genet.* **8**, e1002880 (2012). doi: [10.1371/journal.pgen.1002880](https://doi.org/10.1371/journal.pgen.1002880); pmid: [22912597](https://pubmed.ncbi.nlm.nih.gov/22912597/)
  27. R. Wang, M. Estelle, Diversity and specificity: Auxin perception and signaling through the TIR1/AFB pathway. *Curr. Opin. Plant Biol.* **21**, 51–58 (2014). doi: [10.1016/j.pbi.2014.06.006](https://doi.org/10.1016/j.pbi.2014.06.006); pmid: [25032902](https://pubmed.ncbi.nlm.nih.gov/25032902/)
  28. L. Zhang, J. D. Ward, Z. Cheng, A. F. Dernburg, The auxin-inducible degradation (AID) system enables versatile conditional protein depletion in *C. elegans*. *Development* **142**, 4374–4384 (2015). doi: [10.1242/dev.129635](https://doi.org/10.1242/dev.129635); pmid: [26552885](https://pubmed.ncbi.nlm.nih.gov/26552885/)
  29. T. Negishi, M. Asakawa, M. Kanemaki, H. Sawa, Modified auxin improves the auxin-inducible degradation (AID) system for laid *C. elegans* embryos. *MicroPubl. Biol.* **2019**, (2019). doi: [10.17912/micropub.biology.000190](https://doi.org/10.17912/micropub.biology.000190); pmid: [32550445](https://pubmed.ncbi.nlm.nih.gov/32550445/)
  30. H. Yu et al., Untethering the TIR1 auxin receptor from the SCF complex increases its stability and inhibits auxin response. *Nat. Plants* **1**, 14030 (2015). doi: [10.1038/nplants.2014.30](https://doi.org/10.1038/nplants.2014.30); pmid: [26236497](https://pubmed.ncbi.nlm.nih.gov/26236497/)
  31. W. Zhao et al., A chemically induced proximity system engineered from the plant auxin signaling pathway. *Chem. Sci.* **9**, 5822–5827 (2018). doi: [10.1039/C8SC0235K](https://doi.org/10.1039/C8SC0235K); pmid: [30079194](https://pubmed.ncbi.nlm.nih.gov/30079194/)
  32. D. M. Spencer, T. J. Wandless, S. L. Schreiber, G. R. Crabtree, Controlling signal transduction with synthetic ligands. *Science* **262**, 1019–1024 (1993). doi: [10.1126/science.7694365](https://doi.org/10.1126/science.7694365)
  33. T. Inoue, W. D. Heo, J. S. Grimley, T. J. Wandless, T. Meyer, An inducible translocation strategy to rapidly activate and inhibit small GTPase signaling pathways. *Nat. Methods* **2**, 415–418 (2005). doi: [10.1038/nmeth763](https://doi.org/10.1038/nmeth763); pmid: [15908919](https://pubmed.ncbi.nlm.nih.gov/15908919/)
  34. B.-C. Suh, T. Inoue, T. Meyer, B. Hille, Rapid chemically induced changes of Ptlns(4,5)P<sub>2</sub> gate KCNQ ion channels. *Science* **314**, 1454–1457 (2006). doi: [10.1126/science.1131163](https://doi.org/10.1126/science.1131163); pmid: [16990515](https://pubmed.ncbi.nlm.nih.gov/16990515/)
  35. T. Komatsu et al., Organelle-specific, rapid induction of molecular activities and membrane tethering. *Nat. Methods* **7**, 206–208 (2010). doi: [10.1038/nmeth.1428](https://doi.org/10.1038/nmeth.1428); pmid: [2054678](https://pubmed.ncbi.nlm.nih.gov/2054678)
  36. M. Putrynski, C. Schultz, Protein translocation as a tool: The current rapamycin story. *FEBS Lett.* **586**, 2097–2105 (2012). doi: [10.1016/j.febslet.2012.04.061](https://doi.org/10.1016/j.febslet.2012.04.061); pmid: [22584056](https://pubmed.ncbi.nlm.nih.gov/22584056/)
  37. R. DeRose, T. Miyamoto, T. Inoue, Manipulating signaling at will: Chemically-inducible dimerization (CID) techniques resolve problems in cell biology. *Pflügers Arch.* **465**, 409–417 (2013). doi: [10.1007/s00424-012-1208-6](https://doi.org/10.1007/s00424-012-1208-6); pmid: [23299847](https://pubmed.ncbi.nlm.nih.gov/23299847/)
  38. H. D. Wu et al., Rational design and implementation of a chemically inducible heterotrimerization system. *Nat. Methods* **17**, 928–936 (2020). doi: [10.1038/s41592-020-0913-x](https://doi.org/10.1038/s41592-020-0913-x); pmid: [32747768](https://pubmed.ncbi.nlm.nih.gov/32747768/)
  39. J. Zielich, S. Mangal, E. Zanin, E. Lambie, Establishment of a CRISPR/Cas9-based strategy for inducible protein dimerization. *MicroPubl. Biol.* **2018**, (2018). doi: [10.17912/W2208R](https://doi.org/10.17912/W2208R); pmid: [32550367](https://pubmed.ncbi.nlm.nih.gov/32550367/)
  40. J. A. Loose, A. Ghazi, Auxin treatment increases lifespan in *Caenorhabditis elegans*. *Biol. Open* **10**, bio058703 (2021). doi: [10.1242/bio.058703](https://doi.org/10.1242/bio.058703); pmid: [34184729](https://pubmed.ncbi.nlm.nih.gov/34184729/)
  41. A. Bhoi, F. Palladino, P. Fabrizio, Auxin confers protection against ER stress in *Caenorhabditis elegans*. *Biol. Open* **10**, bio057992 (2021). doi: [10.1242/bio.057992](https://doi.org/10.1242/bio.057992); pmid: [33495210](https://pubmed.ncbi.nlm.nih.gov/33495210/)
  42. G. Lettre et al., Genome-wide RNAi identifies p53-dependent and -independent regulators of germ cell apoptosis in *C. elegans*. *Cell Death Differ.* **11**, 1198–1203 (2004). doi: [10.1038/sj.cdd.4401488](https://doi.org/10.1038/sj.cdd.4401488); pmid: [15272318](https://pubmed.ncbi.nlm.nih.gov/15272318/)
  43. V. A. Byvaltsev et al., Acridine Orange: A Review of Novel Applications for Surgical Cancer Imaging and Therapy. *Front. Oncol.* **9**, 925 (2019). doi: [10.3389/fonc.2019.00925](https://doi.org/10.3389/fonc.2019.00925); pmid: [31612102](https://pubmed.ncbi.nlm.nih.gov/31612102/)
  44. A. V. Zelenin, *Fluorescent and Luminescent Probes for Biological Activity*, W. T. Mason, Ed. (Academic Press, ed. 2, 1999), pp. 117–135.
  45. C. Liu et al., A cooperative network at the nuclear envelope counteracts LINC-mediated forces during oogenesis in *C. elegans*. *Sci. Adv.* **9**, eabn5709 (2023). doi: [10.1126/sciadv.abn5709](https://doi.org/10.1126/sciadv.abn5709); pmid: [37436986](https://pubmed.ncbi.nlm.nih.gov/37436986/)
  46. A. Gartner, A. J. MacQueen, A. M. Villeneuve, “Methods for Analyzing Checkpoint Responses in *Caenorhabditis elegans*” in *Reviews and Model Systems*, vol. 1 of *Checkpoint Controls and Cancer*, : A. H. Schöthal, Ed. (Humana Press, 2004), pp. 257–274.
  47. G. Velez-Aguilar et al., PLK-1 promotes the merger of the parental genome into a single nucleus by triggering lamina disassembly. *eLife* **9**, e59510 (2020). doi: [10.7554/eLife.59510](https://doi.org/10.7554/eLife.59510); pmid: [33030429](https://pubmed.ncbi.nlm.nih.gov/33030429/)
  48. F. Chen et al., Translocation of *C. elegans* CED-4 to nuclear membranes during programmed cell death. *Science* **287**, 1485–1489 (2000). doi: [10.1126/science.287.5457.1485](https://doi.org/10.1126/science.287.5457.1485); pmid: [10688797](https://pubmed.ncbi.nlm.nih.gov/10688797/)
  49. J. Yuan, H. R. Horvitz, The *Caenorhabditis elegans* cell death gene ced-4 encodes a novel protein and is expressed during the period of extensive programmed cell death. *Development* **116**, 309–320 (1992). doi: [10.1242/dev.12309](https://doi.org/10.1242/dev.12309); pmid: [1286611](https://pubmed.ncbi.nlm.nih.gov/1286611/)
  50. A. J. MacQueen, M. P. Colaiacovo, K. McDonald, A. M. Villeneuve, Synapsis-dependent and -independent mechanisms stabilize homolog pairing during meiotic prophase in *C. elegans*. *Genes Dev.* **16**, 2428–2442 (2002). doi: [10.1101/gad.1011602](https://doi.org/10.1101/gad.1011602); pmid: [12231631](https://pubmed.ncbi.nlm.nih.gov/12231631/)
  51. M. P. Colaiacovo et al., Synaptonemal complex assembly in *C. elegans* is dispensable for loading strand-exchange proteins but critical for proper completion of recombination. *Dev. Cell* **5**, 463–474 (2003). doi: [10.1016/S1534-5807\(03\)00232-6](https://doi.org/10.1016/S1534-5807(03)00232-6); pmid: [12967565](https://pubmed.ncbi.nlm.nih.gov/12967565/)
  52. T. L. Gumienny, E. Lambie, E. Hartwig, H. R. Horvitz, M. O. Hengartner, Genetic control of programmed cell death in the *Caenorhabditis elegans* hermaphrodite germline. *Development* **126**, 1011–1022 (1999). doi: [10.1242/dev.1265.1011](https://doi.org/10.1242/dev.1265.1011); pmid: [9927601](https://pubmed.ncbi.nlm.nih.gov/9927601/)
  53. E. L. Stumper et al., Identification of DSB-1, a protein required for initiation of meiotic recombination in *Caenorhabditis elegans*, illuminates a crossover assurance checkpoint. *PLOS Genet.* **9**, e1003679 (2013). doi: [10.1371/journal.pgen.1003679](https://doi.org/10.1371/journal.pgen.1003679); pmid: [23990794](https://pubmed.ncbi.nlm.nih.gov/23990794/)
  54. S. Rosu et al., The *C. elegans* DSB-2 protein reveals a regulatory network that controls competence for meiotic DSB formation and promotes crossover assurance. *PLOS Genet.* **9**, e1003674 (2013). doi: [10.1371/journal.pgen.1003674](https://doi.org/10.1371/journal.pgen.1003674); pmid: [23950729](https://pubmed.ncbi.nlm.nih.gov/23950729/)
  55. G. Huelgas-Morales, M. Sanders, G. Mekonnen, T. Tsukamoto, D. Greenstein, Decreased mechanotransduction prevents nuclear collapse in a *Caenorhabditis elegans* laminopathy. *Proc. Natl. Acad. Sci. U.S.A.* **117**, 31301–31308 (2020). doi: [10.1073/pnas.201505117](https://doi.org/10.1073/pnas.201505117); pmid: [3229589](https://pubmed.ncbi.nlm.nih.gov/3229589)
  56. U. Wolke, E. A. Jeziut, J. R. Priess, Actin-dependent cytoplasmic streaming in *C. elegans* oogenesis. *Development* **134**, 2227–2236 (2007). doi: [10.1242/dev.004952](https://doi.org/10.1242/dev.004952); pmid: [17507392](https://pubmed.ncbi.nlm.nih.gov/17507392/)
  57. M. Yao et al., Force- and cell state-dependent recruitment of Piezo1 drives focal adhesion dynamics and calcium entry. *Sci. Adv.* **8**, eab01461 (2022). doi: [10.1126/sciadv.ab01461](https://doi.org/10.1126/sciadv.ab01461); pmid: [36351022](https://pubmed.ncbi.nlm.nih.gov/36351022/)
  58. A. Tijore et al., Selective killing of transformed cells by mechanical stretch. *Biomaterials* **275**, 120866 (2021). doi: [10.1016/j.biomaterials.2021.120866](https://doi.org/10.1016/j.biomaterials.2021.120866); pmid: [34044258](https://pubmed.ncbi.nlm.nih.gov/34044258/)
  59. B. Coste et al., Piezo1 and Piezo2 are essential components of distinct mechanically activated cation channels. *Science* **330**, 55–60 (2010). doi: [10.1126/science.1193270](https://doi.org/10.1126/science.1193270); pmid: [20813920](https://pubmed.ncbi.nlm.nih.gov/20813920/)
  60. B. Coste et al., Piezo proteins are pore-forming subunits of mechanically activated channels. *Nature* **483**, 176–181 (2012). doi: [10.1038/nature10812](https://doi.org/10.1038/nature10812); pmid: [22343900](https://pubmed.ncbi.nlm.nih.gov/22343900/)
  61. X. Bai et al., *Caenorhabditis elegans* PIEZO channel coordinates multiple reproductive tissues to govern ovulation. *eLife* **9**, e53603 (2020). doi: [10.7554/eLife.53603](https://doi.org/10.7554/eLife.53603); pmid: [32490809](https://pubmed.ncbi.nlm.nih.gov/32490809/)
  62. J. R. M. Millet, L. O. Romero, J. Lee, B. Bell, V. Vásquez, C. elegans PEZ-01 is a mechanosensitive ion channel involved in food sensation. *J. Gen. Physiol.* **154**, e202112960 (2022). doi: [10.1083/jgp.202112960](https://doi.org/10.1083/jgp.202112960); pmid: [34854875](https://pubmed.ncbi.nlm.nih.gov/34854875/)
  63. R. Syeda et al., Chemical activation of the mechanotransduction channel Piezo1. *eLife* **4**, e07369 (2015). doi: [10.7554/eLife.07369](https://doi.org/10.7554/eLife.07369); pmid: [26001275](https://pubmed.ncbi.nlm.nih.gov/26001275/)
  64. D. J. Wynne, O. Rog, P. M. Carlton, A. F. Dernburg, Dynein-dependent processive chromosome motions promote homologous pairing in *C. elegans* meiosis. *J. Cell Biol.* **196**, 47–64 (2012). doi: [10.1083/jcb.201106022](https://doi.org/10.1083/jcb.201106022); pmid: [22232701](https://pubmed.ncbi.nlm.nih.gov/22232701/)
  65. A. Baudrimont et al., Leptotene/zygote chromosome movement via the SUN/KASH protein bridge in *Caenorhabditis elegans* eggs. *PLOS Genet.* **6**, e1001219 (2010). doi: [10.1371/journal.pgen.1001219](https://doi.org/10.1371/journal.pgen.1001219); pmid: [2124819](https://pubmed.ncbi.nlm.nih.gov/2124819)
  66. A. Penkner et al., The nuclear envelope protein Mafefin/SUN-1 is required for homologous pairing in *C. elegans* meiosis. *Dev. Cell* **12**, 873–885 (2007). doi: [10.1016/j.devcel.2007.05.004](https://doi.org/10.1016/j.devcel.2007.05.004); pmid: [17543861](https://pubmed.ncbi.nlm.nih.gov/17543861/)
  67. S. Giacopazzi, D. Vong, A. Devigne, N. Bhalla, PCH-2 collaborates with CMT-1 to proofread meiotic homolog interactions. *PLOS Genet.* **16**, e1008904 (2020). doi: [10.1371/journal.pgen.1008904](https://doi.org/10.1371/journal.pgen.1008904); pmid: [32730253](https://pubmed.ncbi.nlm.nih.gov/32730253/)
  68. A. E. Russo et al., The conserved AAA ATPase PCH-2 distributes its regulation of meiotic prophase events through multiple meiotic HORMADs in *C. elegans*. *PLOS Genet.* **19**, e1010708 (2023). doi: [10.1371/journal.pgen.1010708](https://doi.org/10.1371/journal.pgen.1010708); pmid: [37058535](https://pubmed.ncbi.nlm.nih.gov/37058535/)

69. A. J. Deshong, A. L. Ye, P. Lamelza, N. Bhalla, A quality control mechanism coordinates meiotic prophase events to promote crossover assurance. *PLOS Genet.* **10**, e1004291 (2014). doi: [10.1371/journal.pgen.1004291](https://doi.org/10.1371/journal.pgen.1004291); pmid: [24762417](https://pubmed.ncbi.nlm.nih.gov/24762417/)
70. E. Herruzo *et al.*, Pch2 orchestrates the meiotic recombination checkpoint from the cytoplasm. *PLOS Genet.* **17**, e1009560 (2021). doi: [10.1371/journal.pgen.1009560](https://doi.org/10.1371/journal.pgen.1009560); pmid: [34260586](https://pubmed.ncbi.nlm.nih.gov/34260586/)
71. X. C. Li, J. C. Schimenti, Mouse pachytene checkpoint 2 (trip13) is required for completing meiotic recombination but not synapsis. *PLOS Genet.* **3**, e130 (2007). doi: [10.1371/journal.pgen.0030130](https://doi.org/10.1371/journal.pgen.0030130); pmid: [17696610](https://pubmed.ncbi.nlm.nih.gov/17696610/)
72. I. Roig *et al.*, Mouse TRIP13/PCH2 is required for recombination and normal higher-order chromosome structure during meiosis. *PLOS Genet.* **6**, e1001062 (2010). doi: [10.1371/journal.pgen.1001062](https://doi.org/10.1371/journal.pgen.1001062); pmid: [20711356](https://pubmed.ncbi.nlm.nih.gov/20711356/)
73. Z. Zhang *et al.*, Bi-allelic Missense Pathogenic Variants in TRIP13 Cause Female Infertility Characterized by Oocyte Maturation Arrest. *Am. J. Hum. Genet.* **107**, 15–23 (2020). doi: [10.1016/j.ajhg.2020.05.001](https://doi.org/10.1016/j.ajhg.2020.05.001); pmid: [32473092](https://pubmed.ncbi.nlm.nih.gov/32473092/)
74. J. Y. Chotiner *et al.*, TRIP13 localizes to synapsed chromosomes and functions as a dosage-sensitive regulator of meiosis. *eLife* **12**, RP92195 (2024). doi: [10.7554/eLife.92195](https://doi.org/10.7554/eLife.92195); pmid: [39207914](https://pubmed.ncbi.nlm.nih.gov/39207914/)
75. B. Z. Stanton, E. J. Chory, G. R. Crabtree, Chemically induced proximity in biology and medicine. *Science* **359**, eaao5902 (2018). doi: [10.1126/science.aao5902](https://doi.org/10.1126/science.aao5902); pmid: [29590011](https://pubmed.ncbi.nlm.nih.gov/29590011/)
76. X. Liu, A. Ciulli, Proximity-Based Modalities for Biology and Medicine. *ACS Cent. Sci.* **9**, 1269–1284 (2023). doi: [10.1021/acscentsci.3c00395](https://doi.org/10.1021/acscentsci.3c00395); pmid: [37521793](https://pubmed.ncbi.nlm.nih.gov/37521793/)
77. R. Zhu, C. Liu, G. G. Gunderson, Nuclear positioning in migrating fibroblasts. *Semin. Cell Dev. Biol.* **82**, 41–50 (2018). doi: [10.1016/j.semcdb.2017.11.006](https://doi.org/10.1016/j.semcdb.2017.11.006); pmid: [29241691](https://pubmed.ncbi.nlm.nih.gov/29241691/)
78. Y. A. Miroshnikova, S. A. Wickström, Mechanical Forces in Nuclear Organization. *Cold Spring Harb. Perspect. Biol.* **14**, a039685 (2022). doi: [10.1101/cshperspect.a039685](https://doi.org/10.1101/cshperspect.a039685); pmid: [34187806](https://pubmed.ncbi.nlm.nih.gov/34187806/)
79. A. D. Stephens, E. J. Banigan, J. F. Marko, Chromatin's physical properties shape the nucleus and its functions. *Curr. Opin. Cell Biol.* **58**, 76–84 (2019). doi: [10.1016/j.ceb.2019.02.006](https://doi.org/10.1016/j.ceb.2019.02.006); pmid: [30889417](https://pubmed.ncbi.nlm.nih.gov/30889417/)
80. Y. Kalukula, A. D. Stephens, J. Lammerding, S. Gabriele, Mechanics and functional consequences of nuclear deformations. *Nat. Rev. Mol. Cell Biol.* **23**, 583–602 (2022). doi: [10.1038/s41580-022-00480-z](https://doi.org/10.1038/s41580-022-00480-z); pmid: [35513718](https://pubmed.ncbi.nlm.nih.gov/35513718/)
81. M. M. Nava *et al.*, Heterochromatin-Driven Nuclear Softening Protects the Genome against Mechanical Stress-Induced Damage. *Cell* **181**, 800–817.e22 (2020). doi: [10.1016/j.cell.2020.03.052](https://doi.org/10.1016/j.cell.2020.03.052); pmid: [32302590](https://pubmed.ncbi.nlm.nih.gov/32302590/)
82. L. He, M. Ahmad, N. Perrimon, Mechanosensitive channels and their functions in stem cell differentiation. *Exp. Cell Res.* **374**, 259–265 (2019). doi: [10.1016/j.yexcr.2018.11.016](https://doi.org/10.1016/j.yexcr.2018.11.016); pmid: [30500393](https://pubmed.ncbi.nlm.nih.gov/30500393/)
83. N. Itano, S. Okamoto, D. Zhang, S. A. Lipton, E. Ruoslahti, Cell spreading controls endoplasmic and nuclear calcium: A physical gene regulation pathway from the cell surface to the nucleus. *Proc. Natl. Acad. Sci. U.S.A.* **100**, 5181–5186 (2003). doi: [10.1073/pnas.0531397100](https://doi.org/10.1073/pnas.0531397100); pmid: [12702768](https://pubmed.ncbi.nlm.nih.gov/12702768/)
84. A. G. Prat, H. F. Cantillo, Nuclear ion channel activity is regulated by actin filaments. *Am. J. Physiol.* **270**, C1532–C1543 (1996). doi: [10.1152/ajpcell.1996.270.5.C1532](https://doi.org/10.1152/ajpcell.1996.270.5.C1532); pmid: [8967456](https://pubmed.ncbi.nlm.nih.gov/8967456/)
85. J. Wang *et al.*, Tethering Piezo channels to the actin cytoskeleton for mechanogating via the cadherin- $\beta$ -catenin mechanotransduction complex. *Cell Rep.* **38**, 110342 (2022). doi: [10.1016/j.celrep.2022.110342](https://doi.org/10.1016/j.celrep.2022.110342); pmid: [35139384](https://pubmed.ncbi.nlm.nih.gov/35139384/)
86. A. H. Lewis, J. Grandi, Mechanical sensitivity of Piezo1 ion channels can be tuned by cellular membrane tension. *eLife* **4**, e12088 (2015). doi: [10.7554/eLife.12088](https://doi.org/10.7554/eLife.12088); pmid: [26464186](https://pubmed.ncbi.nlm.nih.gov/26464186/)
87. G. Hajnóczky, E. Davies, M. Madesh, Calcium signaling and apoptosis. *Biochem. Biophys. Res. Commun.* **304**, 445–454 (2003). doi: [10.1016/S0006-291X\(03\)00616-8](https://doi.org/10.1016/S0006-291X(03)00616-8); pmid: [12729578](https://pubmed.ncbi.nlm.nih.gov/12729578/)
88. A. Danese *et al.*, Cell death as a result of calcium signaling modulation: A cancer-centric prospective. *Biochim. Biophys. Acta Mol. Cell Res.* **1868**, 119061 (2021). doi: [10.1016/j.bbamcr.2021.119061](https://doi.org/10.1016/j.bbamcr.2021.119061); pmid: [33991539](https://pubmed.ncbi.nlm.nih.gov/33991539/)
89. M. W. Berchtold, A. Villalobos, The many faces of calmodulin in cell proliferation, programmed cell death, autophagy, and cancer. *Biochim. Biophys. Acta* **1843**, 398–435 (2014). doi: [10.1016/j.bbamcr.2013.10.021](https://doi.org/10.1016/j.bbamcr.2013.10.021); pmid: [24188867](https://pubmed.ncbi.nlm.nih.gov/24188867/)
90. N. T. Chartier *et al.*, A hydraulic instability drives the cell death decision in the nematode germline. *Nat. Phys.* **17**, 920–925 (2021). doi: [10.1038/s41567-021-01235-x](https://doi.org/10.1038/s41567-021-01235-x); pmid: [34777551](https://pubmed.ncbi.nlm.nih.gov/34777551/)
91. H. J. Kim, C. Liu, A. F. Dernburg, How and Why Chromosomes Interact with the Cytoskeleton during Meiosis. *Genes* **13**, 901 (2022). doi: [10.3390/genes13050901](https://doi.org/10.3390/genes13050901); pmid: [35627285](https://pubmed.ncbi.nlm.nih.gov/35627285/)
92. N. Christophorou *et al.*, Microtubule-driven nuclear rotations promote meiotic chromosome dynamics. *Nat. Cell Biol.* **17**, 1388–1400 (2015). doi: [10.1038/ncb3249](https://doi.org/10.1038/ncb3249); pmid: [26458247](https://pubmed.ncbi.nlm.nih.gov/26458247/)
93. A. Viera *et al.*, CDK2 regulates nuclear envelope protein dynamics and telomere attachment in mouse meiotic prophase. *J. Cell Sci.* **128**, 88–99 (2015). doi: [10.1242/jcs.154922](https://doi.org/10.1242/jcs.154922); pmid: [25380821](https://pubmed.ncbi.nlm.nih.gov/25380821/)
94. N. Palmer *et al.*, A novel function for CDK2 activity at meiotic crossover sites. *PLOS Biol.* **18**, e3000903 (2020). doi: [10.1371/journal.pbio.3000903](https://doi.org/10.1371/journal.pbio.3000903); pmid: [33075054](https://pubmed.ncbi.nlm.nih.gov/33075054/)
95. R. Heald, F. McKeon, Mutations of phosphorylation sites in lamin A that prevent nuclear lamina disassembly in mitosis. *Cell* **61**, 579–589 (1990). doi: [10.1016/0092-8674\(90\)90470-Y](https://doi.org/10.1016/0092-8674(90)90470-Y); pmid: [2344612](https://pubmed.ncbi.nlm.nih.gov/2344612/)
96. M. Peter, J. Nakagawa, M. Dorée, J. C. Labbé, E. A. Nigg, In vitro disassembly of the nuclear lamina and M phase-specific phosphorylation of lamins by cdc2 kinase. *Cell* **61**, 591–602 (1990). doi: [10.1016/0092-8674\(90\)90471-P](https://doi.org/10.1016/0092-8674(90)90471-P); pmid: [2188731](https://pubmed.ncbi.nlm.nih.gov/2188731/)
97. G. E. Ward, M. W. Kirschner, Identification of cell cycle-regulated phosphorylation sites on nuclear lamin C. *Cell* **61**, 561–577 (1990). doi: [10.1016/0092-8674\(90\)90469-U](https://doi.org/10.1016/0092-8674(90)90469-U); pmid: [2188730](https://pubmed.ncbi.nlm.nih.gov/2188730/)
98. S. Jeong *et al.*, Cyclin-dependent kinase 1 depolymerizes nuclear lamin filaments by disrupting the head-to-tail interaction of the lamin central rod domain. *J. Biol. Chem.* **298**, 102256 (2022). doi: [10.1016/j.jbc.2022.102256](https://doi.org/10.1016/j.jbc.2022.102256); pmid: [35839855](https://pubmed.ncbi.nlm.nih.gov/35839855/)
99. B. Liebe *et al.*, Mutations that affect meiosis in male mice influence the dynamics of the mid-preleptotene and bouquet stages. *Exp. Cell Res.* **312**, 3768–3781 (2006). doi: [10.1016/j.yexcr.2006.07.019](https://doi.org/10.1016/j.yexcr.2006.07.019); pmid: [17010969](https://pubmed.ncbi.nlm.nih.gov/17010969/)
100. B. Liebe, M. Alsheimer, C. Höög, R. Benavente, H. Scherthan, Telomere attachment, meiotic chromosome condensation, pairing, and bouquet stage duration are modified in spermatocytes lacking axial elements. *Mol. Biol. Cell* **15**, 827–837 (2004). doi: [10.1091/mbc.e03-07-0524](https://doi.org/10.1091/mbc.e03-07-0524); pmid: [14657244](https://pubmed.ncbi.nlm.nih.gov/14657244/)
101. J. Link *et al.*, The meiotic nuclear lamina regulates chromosome dynamics and promotes efficient homologous recombination in the mouse. *PLOS Genet.* **9**, e1003261 (2013). doi: [10.1371/journal.pgen.1003261](https://doi.org/10.1371/journal.pgen.1003261); pmid: [23382700](https://pubmed.ncbi.nlm.nih.gov/23382700/)
102. M. Zhang, *Encyclopedia of Reproduction*, M. K. Skinner, Ed. (Academic Press, ed. 2, 2018), pp. 153–158.
103. Y. Tsatskis *et al.*, The NEMP family supports metazoan fertility and nuclear envelope stiffness. *Sci. Adv.* **6**, eabb4591 (2020). doi: [10.1126/sciadv.abb4591](https://doi.org/10.1126/sciadv.abb4591); pmid: [32923640](https://pubmed.ncbi.nlm.nih.gov/32923640/)
104. A. Biswas, B. H. Ng, V. S. O. Prabhakaran, C. J. Chan, Squeezing the eggs to grow: The mechanobiology of mammalian folliculogenesis. *Front. Cell Dev. Biol.* **10**, 1038107 (2022). doi: [10.3389/fcell.2022.1038107](https://doi.org/10.3389/fcell.2022.1038107); pmid: [36531957](https://pubmed.ncbi.nlm.nih.gov/36531957/)
105. G. Nagamatsu, S. Shimamoto, N. Hamazaki, Y. Nishimura, K. Hayashi, Mechanical stress accompanied with nuclear rotation is involved in the dormant state of mouse oocytes. *Sci. Adv.* **5**, eaav9960 (2019). doi: [10.1126/sciadv.aav9960](https://doi.org/10.1126/sciadv.aav9960); pmid: [31249869](https://pubmed.ncbi.nlm.nih.gov/31249869/)
106. M. Uhlén *et al.*, Proteomics. Tissue-based map of the human proteome. *Science* **347**, 1260419 (2015). doi: [10.1126/science.1260419](https://doi.org/10.1126/science.1260419); pmid: [25613900](https://pubmed.ncbi.nlm.nih.gov/25613900/)
107. S. Brenner, The genetics of *Caenorhabditis elegans*. *Genetics* **77**, 71–94 (1974). doi: [10.1093/genetics/77.1.71](https://doi.org/10.1093/genetics/77.1.71); pmid: [4366476](https://pubmed.ncbi.nlm.nih.gov/4366476/)
108. Y. de la Guardia *et al.*, Run-on of germline apoptosis promotes gonad senescence in *C. elegans*. *Oncotarget* **7**, 39082–39096 (2016). doi: [10.18632/oncotarget.9681](https://doi.org/10.18632/oncotarget.9681); pmid: [27256978](https://pubmed.ncbi.nlm.nih.gov/27256978/)
109. R. S. Kamath, J. Ahringer, Genome-wide RNAi screening in *Caenorhabditis elegans*. *Methods* **30**, 313–321 (2003). doi: [10.1016/S1046-2023\(03\)00050-1](https://doi.org/10.1016/S1046-2023(03)00050-1); pmid: [12828945](https://pubmed.ncbi.nlm.nih.gov/12828945/)
110. R. S. Kamath *et al.*, Systematic functional analysis of the *Caenorhabditis elegans* genome using RNAi. *Nature* **421**, 231–237 (2003). doi: [10.1038/nature01278](https://doi.org/10.1038/nature01278); pmid: [12529635](https://pubmed.ncbi.nlm.nih.gov/12529635/)
111. E. Z. Aprison, S. Dzitoyeva, D. Angeles-Alborea, I. Ruvinsky, A male pheromone that improves the quality of the oogenic germline. *Proc. Natl. Acad. Sci. U.S.A.* **119**, e2015576119 (2022). doi: [10.1073/pnas.2015576119](https://doi.org/10.1073/pnas.2015576119); pmid: [35576466](https://pubmed.ncbi.nlm.nih.gov/35576466/)
112. C. M. Phillips, K. L. McDonald, A. F. Dernburg, "Cytological Analysis of Meiosis in *Caenorhabditis elegans*" in *Cytological Methods*, vol. 2 of *Meiosis*, S. Keeney, Ed. (Humana Press, 2009), pp. 171–195.
113. A. J. MacQueen *et al.*, Chromosome sites play dual roles to establish homologous synapsis during meiosis in *C. elegans*. *Cell* **123**, 1037–1050 (2005). doi: [10.1016/j.cell.2005.09.034](https://doi.org/10.1016/j.cell.2005.09.034); pmid: [16360034](https://pubmed.ncbi.nlm.nih.gov/16360034/)
114. V. Venturini *et al.*, The nucleus measures shape changes for cellular proprioception to control dynamic cell behavior. *Science* **370**, eaba2644 (2020). doi: [10.1126/science.aba2644](https://doi.org/10.1126/science.aba2644); pmid: [33060331](https://pubmed.ncbi.nlm.nih.gov/33060331/)

**ACKNOWLEDGMENTS**

We thank members of the Dernburg Laboratory for stimulating discussions. We thank Z. Lung and X. Liu for their assistance. We thank V. Jantsch, X. Bai, A. Golden, N. Bhalla, Y. Gruenbaum, and Y. Kim for reagents and advice. We also thank A. Villeneuve, O. Rog, D. Starr, R. Bohn, A. Gladfelter, D. Kiehart, K. Liu, M. Wolfner, R. Heald, G. Karpen, S. Lewis, M.-m. Fu, and M. Welch for helpful discussions. We are particularly grateful to Y. He for advice on quantification. Some *C. elegans* strains used in this work were provided by the Caenorhabditis Genetics Center, which is funded by the NIH Office of Research Infrastructure Programs (P40 OD010440). **Funding:** This research was supported by the Life Sciences Research Foundation (C.L.) and the Howard Hughes Medical Institute (A.F.D.). **Author contributions:** Conceptualization: C.L. and A.F.D. Methodology: C.L. and A.F.D. Investigation: C.L. and A.F.D. Visualization: C.L. Supervision: A.F.D. Project administration: A.F.D. Writing – original draft: C.L. Writing – review and editing: C.L. and A.F.D. Funding acquisition: C.L. and A.F.D. **Competing interests:** The authors declare that they have no competing interests. **Data and materials availability:** All data are available in the manuscript or the supplementary materials. Strains generated in this study can be provided upon request. **License information:** Copyright © 2024 the authors, some rights reserved; exclusive licensee American Association for the Advancement of Science. No claim to original US government works. <https://www.science.org/about/science-licenses-journal-article-reuse>

**SUPPLEMENTARY MATERIALS**[science.org/doi/10.1126/science.adm7969](https://science.org/doi/10.1126/science.adm7969)

Materials and Methods

Figs. S1 to S14

Tables S1 to S5

References (115–121)

Movies S1 and S2

Data S1

MDAR Reproducibility Checklist

Submitted 6 November 2023; accepted 20 September 2024

10.1126/science.adm7969